

# Integrin-mediated type II TGF- $\beta$ receptor tyrosine dephosphorylation controls SMAD-dependent profibrotic signaling

Xiwu Chen,<sup>1</sup> Hongtao Wang,<sup>1,2</sup> Hong-Jun Liao,<sup>1</sup> Wen Hu,<sup>1</sup> Leslie Gewin,<sup>1,3</sup> Glenda Mernaugh,<sup>1</sup> Sheng Zhang,<sup>4</sup> Zhong-Yin Zhang,<sup>4</sup> Lorenzo Vega-Montoto,<sup>1</sup> Roberto M. Vanacore,<sup>1</sup> Reinhard Fässler,<sup>5</sup> Roy Zent,<sup>1,6</sup> and Ambra Pozzi<sup>1,6</sup>

<sup>1</sup>Department of Medicine, Division of Nephrology, Vanderbilt University, Nashville, Tennessee, USA. <sup>2</sup>Department of Burn and Cutaneous Surgery, Xijing Hospital, Fourth Military Medical University, Xi'an, China. <sup>3</sup>Department of Research, Veterans Affairs Hospital, Nashville, Tennessee, USA. <sup>4</sup>Department of Biochemistry and Molecular Biology, Indiana University, Indianapolis, Indiana, USA.

<sup>5</sup>Department of Molecular Medicine, Max Planck Institute of Biochemistry, Martinsried, Germany. <sup>6</sup>Department of Medicine, Veterans Affairs Hospital, Nashville, Tennessee, USA.

**Tubulointerstitial fibrosis underlies all forms of end-stage kidney disease. TGF- $\beta$  mediates both the development and the progression of kidney fibrosis through binding and activation of the serine/threonine kinase type II TGF- $\beta$  receptor (T $\beta$ RII), which in turn promotes a T $\beta$ RI-mediated SMAD-dependent fibrotic signaling cascade. Autophosphorylation of serine residues within T $\beta$ RII is considered the principal regulatory mechanism of T $\beta$ RII-induced signaling; however, there are 5 tyrosine residues within the cytoplasmic tail that could potentially mediate T $\beta$ RII-dependent SMAD activation. Here, we determined that phosphorylation of tyrosines within the T $\beta$ RII tail was essential for SMAD-dependent fibrotic signaling within cells of the kidney collecting duct. Conversely, the T cell protein tyrosine phosphatase (TCPTP) dephosphorylated T $\beta$ RII tail tyrosine residues, resulting in inhibition of T $\beta$ R-dependent fibrotic signaling. The collagen-binding receptor integrin  $\alpha$ 1 $\beta$ 1 was required for recruitment of TCPTP to the T $\beta$ RII tail, as mice lacking this integrin exhibited impaired TCPTP-mediated tyrosine dephosphorylation of T $\beta$ RII that led to severe fibrosis in a unilateral ureteral obstruction model of renal fibrosis. Together, these findings uncover a crosstalk between integrin  $\alpha$ 1 $\beta$ 1 and T $\beta$ RII that is essential for T $\beta$ RII-mediated SMAD activation and fibrotic signaling pathways.**

## Introduction

Fibrosis is characterized by the uncontrolled deposition of extracellular matrix components after tissue injury and is the hallmark of many chronic diseases. Fibrosis is irreversible and disrupts the normal tissue architecture, eventually leading to organ dysfunction and failure. Although fibrosis is promoted by a range of different factors, including genetic predisposition, cytokines, matrix receptors, and oxidative stress (1), an accepted treatment is still not available. Thus, there is great interest in deciphering the molecular mechanisms controlling matrix homeostasis in normal and pathological states in order to devise effective therapies.

Growth factors and cytokines are important regulators of matrix homeostasis (1, 2). The cytokine TGF- $\beta$  is one of the most potent stimulators of fibrosis following chronic injury. TGF- $\beta$  exerts its functions by binding of the constitutively active type II TGF- $\beta$  receptor (T $\beta$ RII), which leads to serine phosphorylation and activation of T $\beta$ RI (also known as ALK5). The activated T $\beta$ RI, in turn, promotes serine phosphorylation of SMAD2 and SMAD3, their association with SMAD4, translocation to the nucleus, and transcription of profibrotic genes (3, 4). Signaling from T $\beta$ RII to T $\beta$ RI is primarily modulated by the autophosphorylation of 3 serine residues in the T $\beta$ RII cytoplasmic tail: S213 and S409 promote kinase activity and interaction with T $\beta$ RI, while S416 inhibits the

receptor (5). The T $\beta$ RII cytoplasmic domain also contains 5 phosphorylatable tyrosines: Y259, Y284, Y336, Y424, and Y470 (6, 7). T $\beta$ RIIY284 was shown to be phosphorylated by Src and implicated in T $\beta$ R-mediated noncanonical p38 MAPK activation (7). Whether the remaining tyrosine residues are also involved in signaling and control T $\beta$ RII-mediated SMAD activation and fibrotic signaling is currently unknown.

Integrins are also potent regulators of matrix homeostasis (1, 2). They are transmembrane receptors for extracellular matrix components formed by 2 noncovalently associated  $\alpha$  and  $\beta$  subunits. In mammalian cells, integrins combine to form 24 different heterodimers with different ligand specificity to matrix molecules (8). Upon ligand binding, integrins initiate multiple intracellular signaling pathways that regulate critical cellular functions such as migration, survival, and proliferation (9). Integrins also regulate matrix homeostasis by modulating matrix expression and degradation, altering the activation of specific receptor tyrosine kinases, or controlling the activation and levels of growth factors like TGF- $\beta$  (10). In this context, integrins  $\alpha$ v $\beta$ 6 and  $\alpha$ v $\beta$ 8 regulate the release of TGF- $\beta$  from its latency-associated protein and its ability to interact with T $\beta$ Rs on nearby cells (11–13). Furthermore, activation of integrin  $\alpha$ v $\beta$ 3 enhances TGF- $\beta$ -mediated collagen synthesis (14), whereas integrin  $\alpha$ 2 $\beta$ 1 inhibits TGF- $\beta$ -mediated functions by downregulating TGF- $\beta$  synthesis (15). Finally, integrin  $\alpha$ v $\beta$ 3 can also potentiate TGF- $\beta$  signaling by controlling the activation state of T $\beta$ RII. This is achieved through a direct interaction of integrin  $\beta$ 3 and T $\beta$ RII (16) that enables Src to phosphorylate T $\beta$ RIIY284.

**Conflict of interest:** The authors have declared that no conflict of interest exists.

**Submitted:** June 19, 2013; **Accepted:** May 21, 2014.

**Reference information:** *J Clin Invest*. 2014;124(8):3295–3310. doi:10.1172/JCI171668.

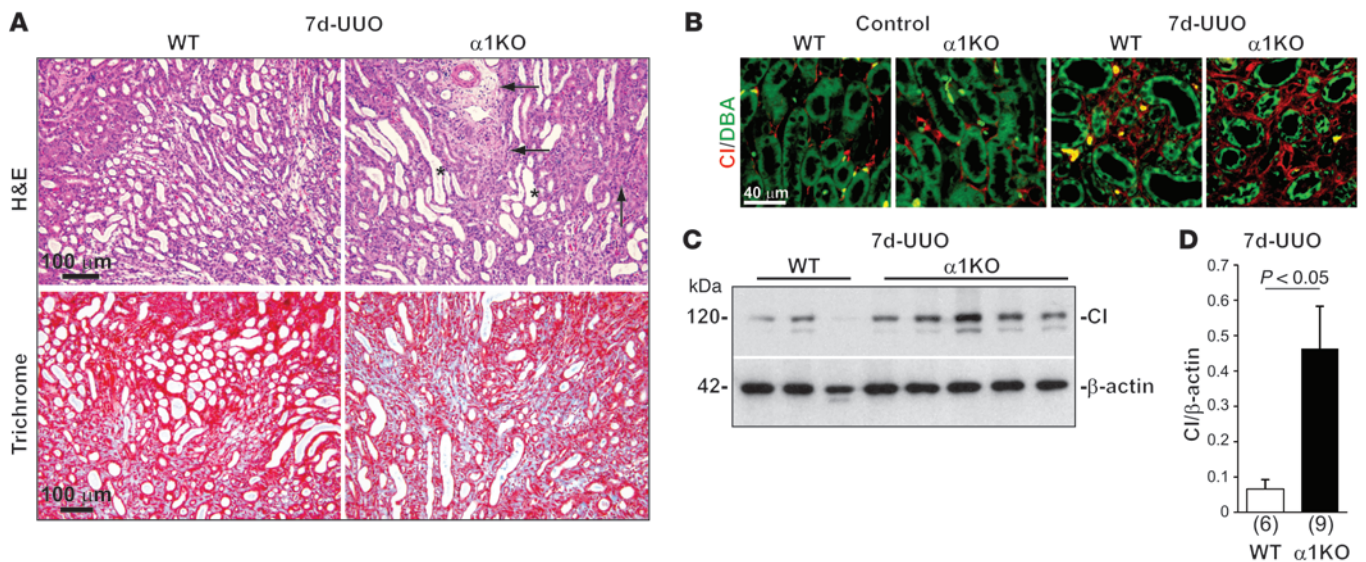


**Figure 1. Loss of integrin  $\alpha 1\beta 1$  leads to exacerbated fibrosis following UUU.** (A) H&E and Trichrome staining of kidneys from WT and  $\alpha 1$ KO mice 7 days after UUU, showing more dilated tubules (asterisks), fibrosis (arrows), and collagen deposition (blue staining) in the injured  $\alpha 1$ KO mice. (B) Paraffin kidney sections from control and injured mice were stained with FITC-conjugated DBA (green) and collagen I (Cl; red) antibodies to visualize CDs and degree of fibrosis, respectively. Increased deposition of collagen was evident in the injured  $\alpha 1$ KO mice. (C) Kidney lysates (20  $\mu$ g/lane) from injured WT and  $\alpha 1$ KO mice ( $n = 3$  and 5 shown, respectively) were analyzed by Western blot for levels of collagen I. (D) Collagen I and  $\beta$ -actin bands were quantified by densitometry analysis, and collagen I signal was expressed as the collagen I/ $\beta$ -actin ratio. Values are mean  $\pm$  SEM of the indicated  $n$ . Scale bars: 100  $\mu$ m (A); 40  $\mu$ m (B).

This in turn leads to activation of p38 MAPK, induction of epithelial-to-mesenchymal transition (EMT), proliferation, and invasion of breast cancer epithelial cells (7, 16). Whether integrins also alter TGF- $\beta$  profibrotic signaling by directly regulating the activity of the T $\beta$ R complex is currently unknown.

Tubulointerstitial fibrosis is the hallmark of all forms of end-stage kidney disease. In mice, the unilateral ureteral obstruction (UUO) model recapitulates all the key features of the typical fibrogenic response, including excess matrix accumulation, influx of inflammatory cells, and increased synthesis of profibrotic molecules such as TGF- $\beta$  (17). This injury model was used to define the protective effects of deleting integrin  $\beta 6$  due to reduced local activation of TGF- $\beta$  (18) and the profibrotic effect of deleting integrin  $\beta 1$  in collecting duct (CD) cells (the primary cellular target of UUO-mediated injury) due to impaired growth factor signaling (19).

The major collagen-binding receptor integrin  $\alpha 1\beta 1$  is expressed in kidney glomerular and CD cells (20, 21). Integrin  $\alpha 1\beta 1$  negatively regulates collagen synthesis by sensing extracellular collagen levels and downregulating endogenous collagen synthesis (22). Consistent with these findings, integrin  $\alpha 1$ -null mice develop severe kidney glomerular injury due to increased production of reactive oxygen species and synthesis of glomerular collagen (21, 23). Integrin  $\alpha 1\beta 1$  decreases production of reactive oxygen species by downregulating the activation state of the profibrotic EGF receptor. This is achieved by controlling the level and phosphorylation state of caveolin-1, a scaffolding protein involved in receptor signaling and localization, as well as the activation state of the T cell protein tyrosine phosphatase (TCPTP) (24–26). While the contribution of the integrin  $\alpha 1\beta 1$ /TCPTP axis to glomerular injury has been widely investigated, how this com-

plex contributes to kidney tubular injury is currently unknown. Here we showed that integrin  $\alpha 1\beta 1$  negatively regulated UUO-mediated tubulointerstitial fibrosis by a novel mechanism involving TCPTP-mediated downregulation of tyrosine phosphorylation levels of the cytoplasmic tail of T $\beta$ R $II$  and consequent dampening of SMAD-dependent profibrotic signaling.

## Results

**Increased UUO-mediated collagen I production in integrin  $\alpha 1$ -null mice.** Since it is not known whether the collagen-binding receptor integrin  $\alpha 1\beta 1$  mediates kidney tubulointerstitial fibrosis, we performed UUO in BALB/c WT and integrin  $\alpha 1$ -null (*Itga1*<sup>-/-</sup>; referred to herein as  $\alpha 1$ KO) male mice. This experiment revealed that  $\alpha 1$ KO mice developed more severe injury than WT mice 7 days after UUO, which was characterized by worse tubular dilatation and matrix deposition as well as increased collagen I levels in the kidney medulla and the whole kidney (Figure 1, A–D).

**Altered epithelial cell morphology in  $\alpha 1$ KO CD cells.** Tubular kidney CD cells are the primary cellular target of UUO-mediated injury. Therefore, we generated primary cultures of WT and  $\alpha 1$ KO CD cells (Supplemental Figure 1A; supplemental material available online with this article; doi:10.1172/JCI1668DS1) and examined their contribution to the phenotype of  $\alpha 1$ KO mice. Although the epithelial and CD origin of the  $\alpha 1$ KO CD cells was confirmed by aquaporin-2 expression, they underwent EMT — characterized by a fibroblast-like phenotype, increased levels of  $\alpha$ SMA, and loss of the epithelial markers ZO-1 and E-cadherin — when grown on plastic (Figure 2, A–D). Loss of E-cadherin expression in the  $\alpha 1$ KO CD cells was accompanied by increased levels of ZEB1 (Figure 2D), a suppressor of E-cadherin expression whose levels are positively regulated by TGF- $\beta$  (27, 28).

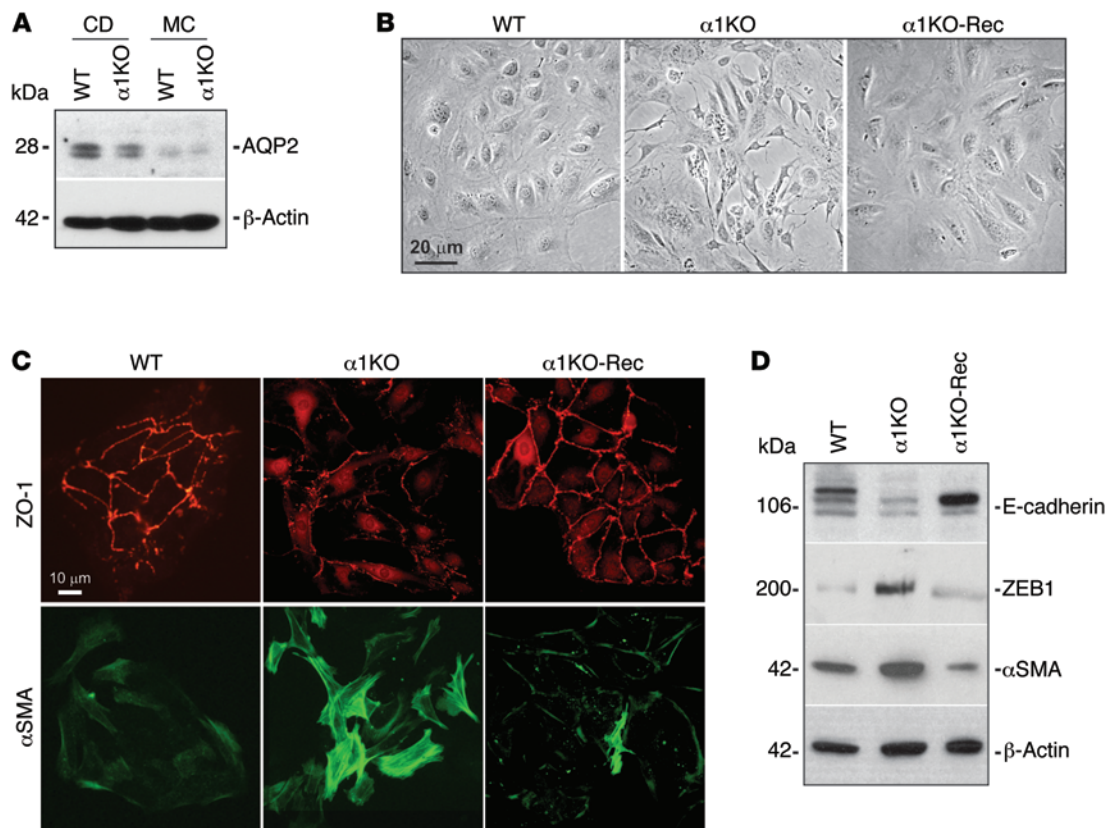


**Figure 2. α1KO CD cells undergo EMT.** (A) Cell lysates (10 μg/lane) from serum-starved WT and α1KO CD cells were analyzed by Western blot for levels of aquaporin-2 (AQP2). Mesangial cells (MC) were used as a negative control. (B) Morphology of WT, α1KO, and α1KO-Rec CD cells grown on plastic. α1KO cells showed a fibroblast-like phenotype relative to the epithelial morphology observed in WT or α1KO-Rec cells. (C) CD cells were stained with anti-ZO-1 and anti-αSMA antibodies to visualize levels and localization of epithelial and myofibroblast markers. (D) Western blot analysis showing loss of epithelial markers (E-cadherin), increased myofibroblast markers (αSMA), and increased levels of E-cadherin suppressors (ZEB1) in α1KO compared with WT or α1KO-Rec CD cells (20 μg/lane cell lysates used for analysis). Scale bars: 20 μm (B); 10 μm (C).

To rule out the possibility that acquisition of mesenchymal characteristics in α1KO CD cells was because the cells were cultured on plastic, freshly isolated WT and α1KO CD cells were grown on transwells. Similar to cells grown on plastic, α1KO CD cells cultured for 3 days on transwells developed a fibroblast-like phenotype, characterized by increased levels of αSMA and loss of the epithelial marker ZO-1 (Supplemental Figure 2, A and B). Importantly, α1KO cells reconstituted with the human integrin α1 subunit cDNA (α1KO-Rec cells; Supplemental Figure 1B) showed a restored WT CD epithelial cell phenotype (Figure 2, B–D), which indicates that the EMT of the α1KO CD cells was caused by loss of integrin α1β1 expression, not by cell culture conditions.

**Loss of integrin α1β1 leads to increased basal levels of activated SMAD2 and SMAD3.** The EMT phenotype of α1KO CD cells resembled that of epithelial cells exposed to TGF-β ligand (29). To determine whether TGF-β pathways were activated in the absence of integrin α1β1, we analyzed the basal levels of activated SMAD2 and SMAD3 in CD cells grown on plastic or transwells and found significantly more phosphorylated SMAD2 (pSMAD2) and pSMAD3 as well as synthesis of collagens I and IV in α1KO versus WT and α1KO-Rec CD cells (Figure 3, A–D, and Supplemental Figure 2, C and D). Altered expression of TβRI and TβRII in the α1KO cells was excluded as the cause of elevated

pSMAD2/3 levels (Figure 3A). In addition, TGF-β-mediated noncanonical signaling was also unaffected in α1KO CD cells (Supplemental Figure 3).

Consistent with our *in vitro* findings, we also detected increased nuclear levels of activated SMAD3 in CD cells of UUO-injured α1KO mice and significantly higher levels of activated SMAD2 and SMAD3 in whole kidney lysates isolated from α1KO mice 7 days after UUO (Figure 3, E–G).

**Blocking TβR signaling rescues the phenotype of α1KO CD cells.** TGF-β signaling is transduced by the serine/threonine kinase receptors TβRI and TβRII. Upon activation by TβRII, TβRI triggers SMAD2 and SMAD3 activation (3, 4). Inhibition of TβR signaling in α1KO CD cells with the TβRI-specific inhibitor SB431542 reverted their EMT phenotype to an epithelial-like morphology, increased membrane localization of ZO-1, and decreased levels of pSMAD2, pSMAD3, αSMA, and collagens I and IV (Figure 4, A–C), which indicates that integrin α1β1 negatively regulates TβR-mediated fibrotic signaling in CD cells.

A possible mechanism for these effects is that loss of integrin α1β1 leads to increased levels of activated TGF-β. Similar levels of total and active TGF-β were detected in kidney lysates from WT and α1KO mice and in conditioned medium from WT and α1KO CD cells (Supplemental Figure 4, A–D), which suggests that

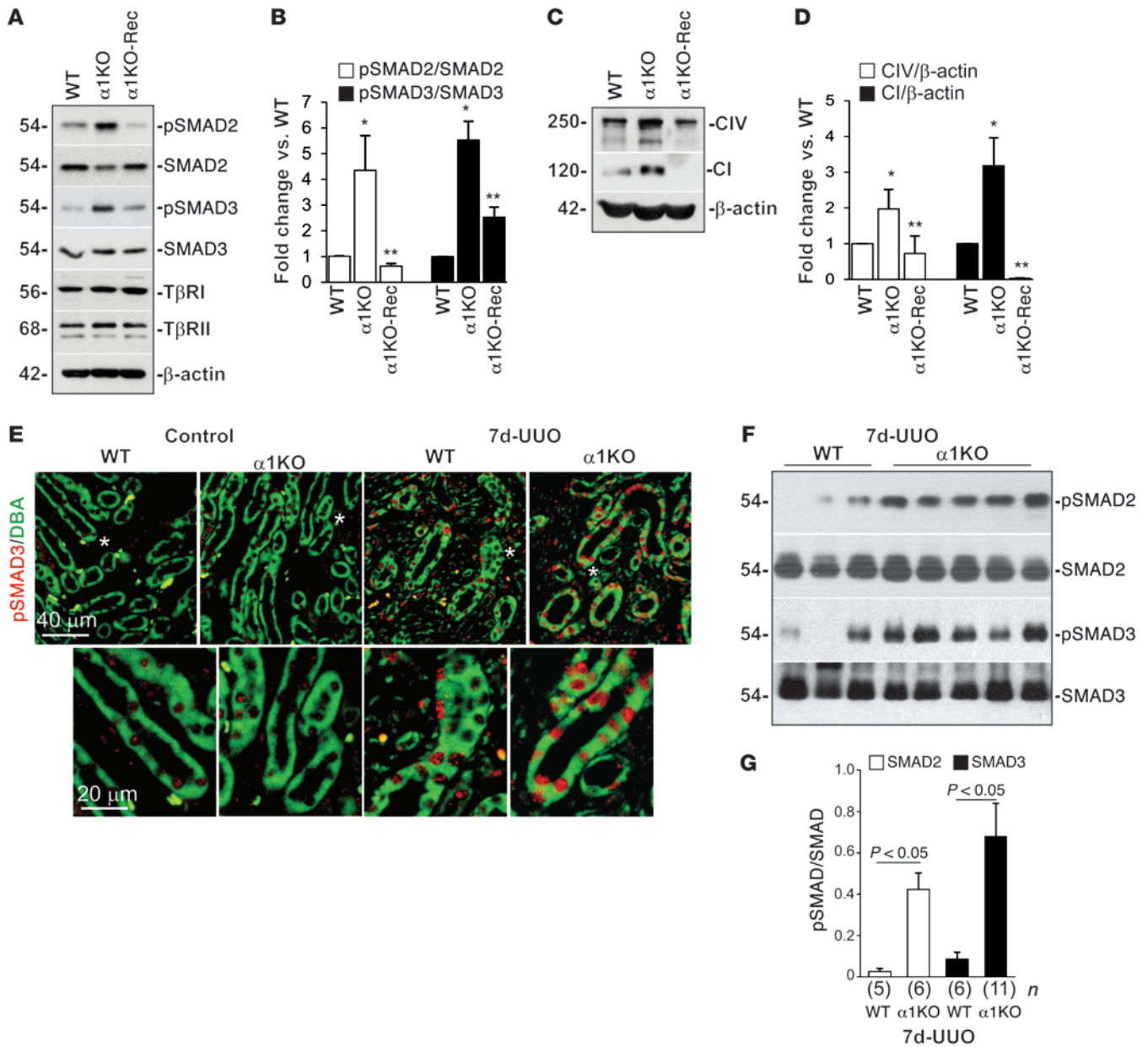


**Figure 3. Increased TGF-β downstream signaling in α1KO CD cells and mice.** (A and C) Cell lysates (20 μg/lane) from the indicated serum-starved cells were analyzed by Western blot for levels of pSMAD2, pSMAD3, TβRI, and TβRII (A) as well as collagens I and IV (C). (B and D) pSMAD2, pSMAD3, SMAD2, and SMAD3 (B) as well as collagen I, collagen IV, and β-actin (D) bands were quantified by densitometry analysis, and signals are expressed as a pSMAD/SMAD or collagen/β-actin ratio. Values are mean ± SEM of 3 independent experiments. \**P* ≤ 0.05 vs. WT; \*\**P* ≤ 0.05 vs. α1KO. (E) Paraffin kidney sections were stained with FITC-conjugated DBA (green) and anti-pSMAD3 (red) antibodies to visualize CDs and activated SMAD3, respectively. (F) Kidney lysates (20 μg/lane) from injured WT and α1KO mice (*n* = 3 and 5 shown, respectively) were analyzed by Western blot for levels of activated and total SMAD2 and SMAD3. (G) pSMAD2, pSMAD3, SMAD2, and SMAD3 bands were quantified by densitometry analysis; signal is expressed as pSMAD/SMAD ratio. Values are mean ± SEM of the indicated *n*. Scale bars: 40 μm (E, top); 20 μm (E, bottom).

increased levels of active TGF-β ligands were not responsible for the EMT phenotype. Furthermore, the normal α1KO CD cell surface expression of integrins involved in regulating levels and/or activation of TGF-β (e.g., integrins α2, αv, β3, and αvβ6; Supplemental Figure 4E) further excluded an increased release of extracellular matrix-bound TGF-β ligand. Moreover, inhibition of TGF-β activity with the pan-TGF-β blocking antibody 2G7 only slightly reduced the elevated levels of activated SMAD3 in α1KO

CD cells (Figure 5A). Together, these findings suggest that the increased TGF-β-mediated signaling in α1KO CD cells is TGF-β ligand independent and thus cell autonomous.

We next compared the ability of WT and α1KO CD cells to respond to TGF-β1; α1KO CD cells showed increased and more sustained SMAD3 activation in response to TGF-β1 compared with that in WT CD cells (Figure 5, B and C). Although both SMAD2 and SMAD3 were phosphorylated in α1KO CD cells, in the following

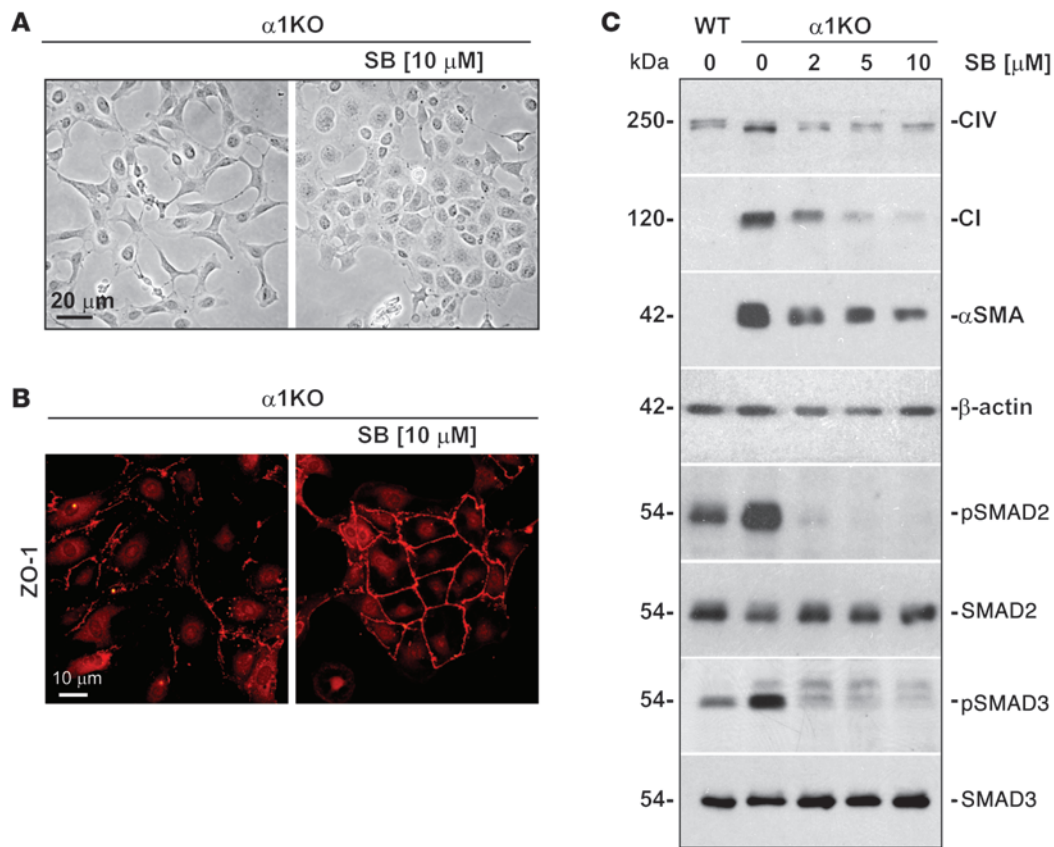


**Figure 4. Inhibition of T $\beta$ R signaling reverts EMT in  $\alpha$ 1KO CD cells.** (A) Morphology of  $\alpha$ 1KO CD cells cultured on plastic in 0.2% serum with or without the T $\beta$ R1 inhibitor SB431542 (SB) for 4 days. (B)  $\alpha$ 1KO CD cells were cultured as in A, then stained with anti-ZO-1 antibodies to visualize its expression and localization. (C) Serum-starved WT and  $\alpha$ 1KO CD cells were treated with SB431542 at the indicated concentrations. After 24 hours, cell lysates (20  $\mu$ g/lane) were analyzed by Western blot for levels of collagen I, collagen IV,  $\alpha$ SMA, pSMAD2, SMAD2, pSMAD3, and SMAD3. Scale bars: 20  $\mu$ m (A); 10  $\mu$ m (B).

experiments we focused on SMAD3, as this transcription factor positively correlates to EMT, matrix accumulation, and renal fibrosis (30).

*T $\beta$ R1I is highly phosphorylated on tyrosines in  $\alpha$ 1KO CD cells.* Integrin  $\alpha$ 1 $\beta$ 1 inhibits the activation and signaling of the EGF receptor by preventing tyrosine phosphorylation of its cytoplasmic tail (25, 31). Therefore, we decided to investigate whether integrin  $\alpha$ 1 $\beta$ 1 can also block TGF- $\beta$  signaling at the receptor level. As the T $\beta$ R1I cytoplasmic tail contains 5 phosphorylatable tyrosines (6, 7), we analyzed basal levels of T $\beta$ R1I tyrosine phosphorylation in serum-starved WT and  $\alpha$ 1KO CD cells. Cell lysates were immunoprecipitated with the anti-phosphotyrosine antibody 4G10 or with IgG isotype controls and subsequently immunoblotted with anti-phosphotyrosine (anti-pY99) or anti-mouse T $\beta$ R1I antibodies. Phosphorylated T $\beta$ R1I was only detectable in samples derived from  $\alpha$ 1KO CD cells (Figure 6A), which suggests that loss of integrin  $\alpha$ 1 $\beta$ 1 expression increases tyrosine phosphorylation of T $\beta$ R1I.

Next we sought to determine whether tyrosine-phosphorylated T $\beta$ R1I increased the phosphorylation/activation of T $\beta$ R1. We analyzed basal levels of T $\beta$ R1 serine and threonine phosphorylation in serum-starved WT and  $\alpha$ 1KO CD cells by immunoprecipitating cell lysates with anti-phosphoserine and anti-phosphothreonine antibodies followed by immunoblotting with either anti-phosphoserine or anti-mouse T $\beta$ R1 antibodies. Increased levels of pT $\beta$ R1

were detectable in samples derived from  $\alpha$ 1KO CD cells (Supplemental Figure 5A), which suggests that increased tyrosine phosphorylation of T $\beta$ R1I indeed leads to increased serine and threonine phosphorylation of T $\beta$ R1.

*The T cell protein tyrosine phosphatase prevents T $\beta$ R1I-mediated EMT.* We next determined the mechanism by which integrin  $\alpha$ 1 $\beta$ 1 inhibits tyrosine phosphorylation of T $\beta$ R1I. We and others have shown that TCPTP binds to the integrin  $\alpha$ 1 cytoplasmic tail, is activated in an integrin  $\alpha$ 1 $\beta$ 1-dependent manner, and dephosphorylates tyrosines both on receptor tyrosine kinases (such as EGF, VEGF, and PDGF receptors) and on scaffolding proteins (such as caveolin-1) (24, 25, 31–33). Interestingly, analysis of the human and mouse T $\beta$ R1I cytoplasmic tails with PhosphoMotif Finder confirmed the presence of 5 potential tyrosine phosphorylation sites (Y259, Y284, Y336, Y424, and Y470) and identified 3 of them (Y284, Y336, and Y470) as substrates for TCPTP dephosphorylation (Supplemental Figure 6, A–C). In support of a role for TCPTP in TGF- $\beta$  signaling, shRNAi-mediated downregulation of TCPTP or treatment with the selective TCPTP inhibitor compound 8 (34) induced EMT of WT CD cells, with increased SMAD3 activation, loss of ZO-1 at the plasma membrane, and increased expression of  $\alpha$ SMA and collagens I and IV, which were efficiently prevented by treatment with the T $\beta$ R1 inhibitor SB431542 (Figure 6, B–F).

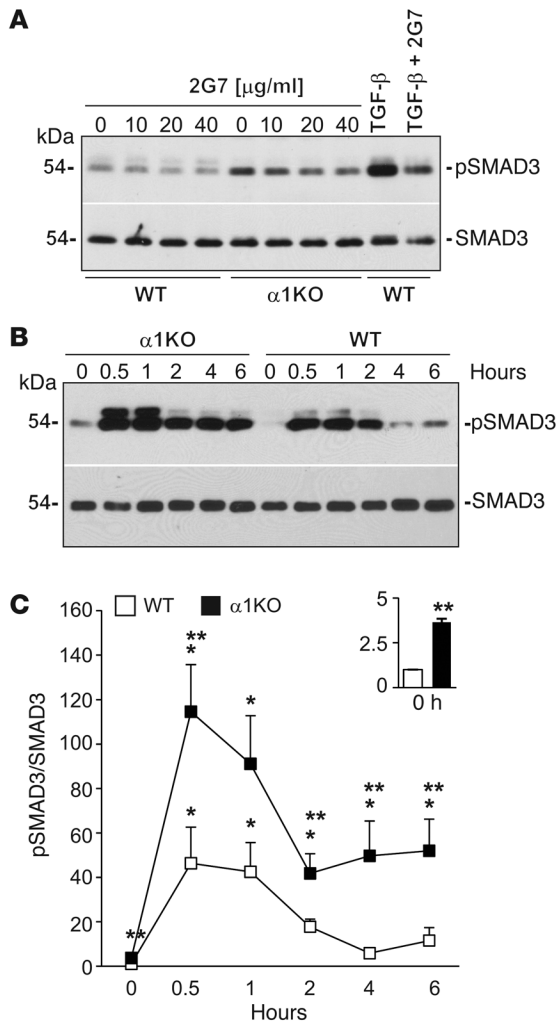


**Figure 5. Prolonged SMAD3 activation in  $\alpha$ 1KO CD cells stimulated with TGF- $\beta$ .** (A) Serum-starved WT and  $\alpha$ 1KO CD cells were treated with the indicated concentrations of the blocking anti-TGF- $\beta$  antibody 2G7. After 24 hours, cell lysates (20  $\mu$ g/lane) were analyzed by Western blot for levels of pSMAD3 and SMAD3. As controls, 24 hour serum-starved WT CD cells with or without 2G7 (40  $\mu$ g/ml) were treated with TGF- $\beta$  (5 ng/ml) 1 hour prior to harvesting. (B) Serum-starved WT and  $\alpha$ 1KO CD cells were treated with TGF- $\beta$  (5 ng/ml) for the times indicated. Cell lysates (20  $\mu$ g/lane) were analyzed by Western blot for levels of pSMAD3 and SMAD3. (C) pSMAD3 and SMAD3 bands were quantified by densitometry analysis, and pSMAD3 signal is expressed as the pSMAD3/SMAD3 ratio. Values are mean  $\pm$  SEM of 3 independent experiments. \* $P$   $\leq$  0.05 vs. untreated; \*\* $P$   $\leq$  0.05 vs. WT.

shRNAi-mediated depletion of TCPTP in WT CD cells also increased serine and threonine phosphorylation of T $\beta$ RI and tyrosine phosphorylation of T $\beta$ RII (Figure 6G and Supplemental Figure 5B), which indicates that TCPTP inhibits T $\beta$ R signaling and EMT of WT CD cells.

We next determined whether TCPTP activation diminishes T $\beta$ R-mediated signaling in  $\alpha$ 1KO CD cells. Activation of TCPTP with the polyamine spermidine (33) in  $\alpha$ 1KO CD cells reverted their fibroblast-like morphology to an epithelial phenotype and decreased basal levels of activated SMAD3 and expression of collagen I (Figure 7, A and B). In addition, immunoprecipitation of lysates of spermidine-treated  $\alpha$ 1KO CD cells with the anti-phosphotyrosine antibody 4G10 failed to immunoprecipitate T $\beta$ RII (Figure 7C), which suggests that spermidine-mediated TCPTP activation decreased tyrosine phosphorylation of T $\beta$ RII.

To confirm the *in vitro* finding and the relevance of TCPTP activation in kidney fibrosis, we treated  $\alpha$ 1KO mice with spermidine at the time of UUO. At 7 days after UUO, we observed a significantly attenuated injury response, characterized by decreased tubular dilatation and tubulointerstitial fibrosis, decreased expression of collagens I and IV, and diminished SMAD3 activation (Figure 7, D–H).

Polyamines such as spermidine and integrin  $\alpha$ 1 $\beta$ 1 regulate macrophage functions and tissue infiltration (35–37). As macro-

phages contribute to UUO-mediated fibrosis, we quantified the number of F4/80-positive cells in the papilla of injured  $\alpha$ 1KO mice untreated or treated with spermidine. Since we found comparable numbers of macrophages in these 2 groups (Supplemental Figure 7), we concluded that the beneficial effects of spermidine are likely due to reduced T $\beta$ R-mediated signaling in resident cells, rather than altered immunological responses.

*Tyrosine phosphatase directly binds and dephosphorylates T $\beta$ RII.* Since TCPTP binds the integrin  $\alpha$ 1 subunit (24, 31) and we observed evidence in support of its role in T $\beta$ RII tyrosine dephosphorylation, we hypothesized that TCPTP, integrin  $\alpha$ 1 $\beta$ 1, and T $\beta$ RII form a ternary protein complex. Immunoprecipitating the integrin  $\alpha$ 1 subunit from lysates of  $\alpha$ 1KO-Rec CD cells and immunoblotting the precipitate with specific antibodies against integrin  $\alpha$ 1, T $\beta$ RII, and TCPTP confirmed that they indeed formed a complex (Supplemental Figure 8A). In addition, immunofluorescence staining performed on frozen sections of human kidneys revealed that integrin  $\alpha$ 1, T $\beta$ RII, and TCPTP colocalized in CDs (Supplemental Figure 8, B–D).

To further confirm that TCPTP can directly bind and dephosphorylate T $\beta$ RII, we performed ELISA using recombinant full-length TCPTP and human glutathione S-transferase–T $\beta$ RII cytoplasmic domain (GST–T $\beta$ RIICD) as well as tyrosine-phosphorylated GST–T $\beta$ RIICD (GST–pYT $\beta$ RIICD) (Supplemental Figure 9, A–C), and *in vitro* dephosphorylation assays with GST–pYT $\beta$ RIICD and a constitutively active form of TCPTP (TCPTP-37). Whereas GST alone showed no binding to TCPTP, GST–T $\beta$ RIICD and GST–pYT $\beta$ RIICD demonstrated robust binding to immobilized TCPTP (Figure 8A). Furthermore, TCPTP-37 efficiently dephosphorylated GST–pYT $\beta$ RIICD in a dose-dependent manner (Figure 8, B and C). Importantly, addition of the phosphatase inhibitor sodium vanadate to the reaction mixture prevented TCPTP-37-mediated GST–pYT $\beta$ RIICD dephosphorylation (Figure 8B), which suggests that T $\beta$ RII is a TCPTP substrate.

As the cytoplasmic domain of T $\beta$ RII contains 3 potential TCPTP dephosphorylatable tyrosines (Y284, Y336, and Y470; Supplemental Figure 6 and Supplemental Figure 9A), we investigated whether these 3 sites can be dephosphorylated by TCPTP *in vitro*. We treated GST–pYT $\beta$ RIICD recombinant proteins carrying the triple Y284/336/470A mutations (GST–pYT $\beta$ RIIY284/336/470ACD) with TCPTP-37. GST–pYT $\beta$ RIIY284/336/470ACD retained a basal tyrosine phosphorylation signal, due to the remaining phosphorylatable sites T $\beta$ RIIY259 and T $\beta$ RIIY424 in the cytoplasmic domain (Figure 8D, Supplemental Figure 6, and Supplemental

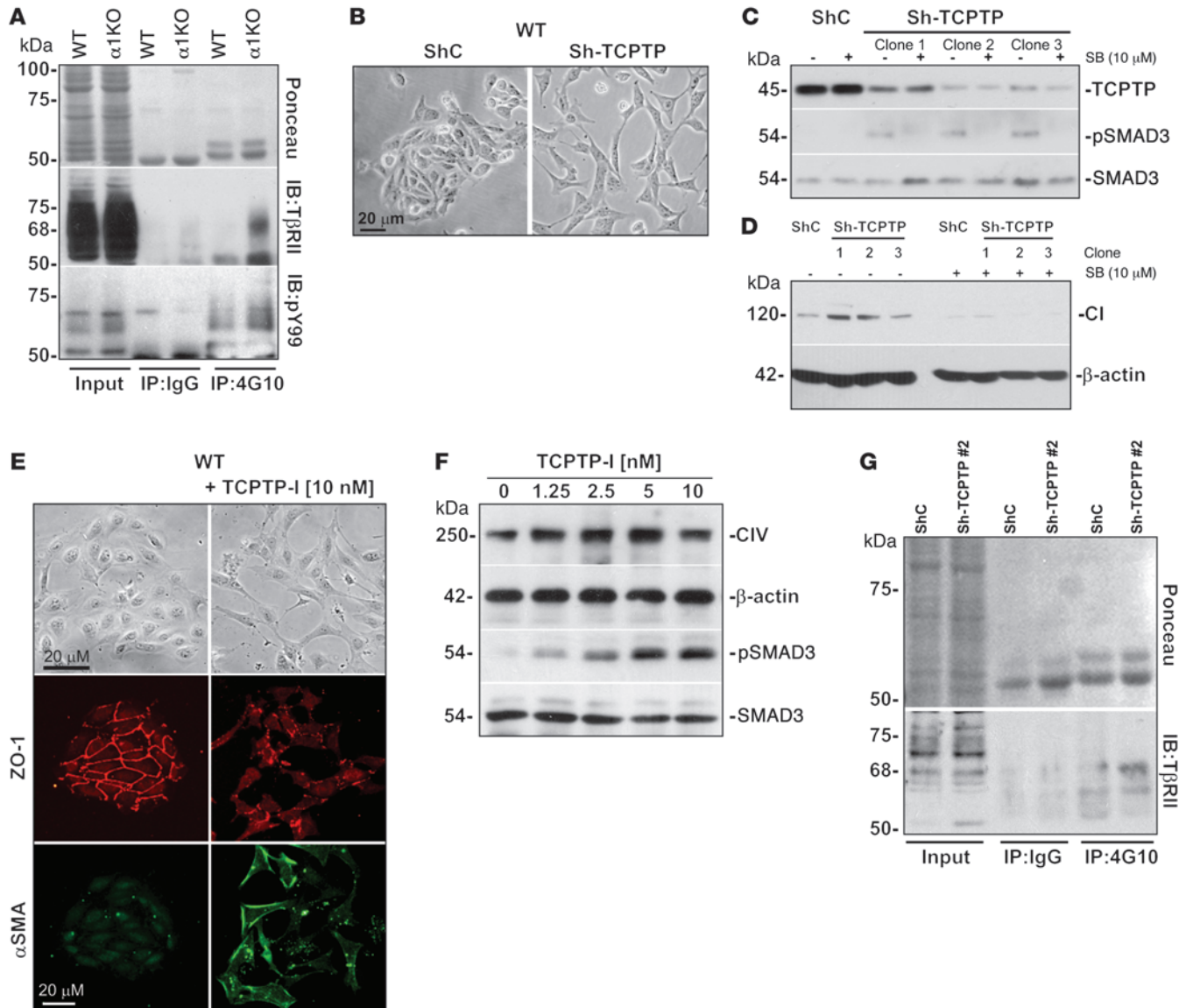


**Figure 6. TCPTP regulates TβRII tyrosine phosphorylation and signaling.** (A) Cell lysates (0.5 mg) from serum-starved WT and α1KO CD cells were immunoprecipitated with the anti-phosphotyrosine antibody 4G10 (10 μg) or with mouse IgG isotype control antibody (10 μg) and analyzed by Western blot. A band corresponding to TβRII (~68 kDa) was visible only in α1KO cells incubated with 4G10. Tyrosine-phosphorylated products (50–100 kDa) were detected with anti-pY99 antibodies in both WT and α1KO CD cells. (B) Morphology of WT CD cells stably transfected with shRNAi control (ShC) or TCPTP shRNAi (Sh-TCPTP). (C and D) Cell lysates (20 μg/lane) from serum-starved WT CD cells transfected with ShC (1 clone shown) or Sh-TCPTP (3 clones shown) and treated with or without SB431542 (SB) were analyzed by Western blot for levels of TCPTP, pSMAD3, SMAD3, and collagen I. (E) WT CD cells were cultured on plastic in 0.2% serum with or without the TCPTP inhibitor compound 8 (TCPTP-I) for 4 days and then stained with anti-ZO-1 and anti-αSMA antibodies. (F) Serum-starved WT CD cells were treated with TCPTP inhibitor at the concentrations indicated. After 24 hours, cell lysates (20 μg/lane) were analyzed for levels of collagen IV, pSMAD3, and SMAD3. (G) Cell lysates (0.5 mg) from serum-starved WT CD cells transfected with control or TCPTP shRNAi (1 clone each shown) were immunoprecipitated and analyzed by Western blot as in A. A band corresponding to TβRII was more evident in lysates of CD cells transfected with TCPTP shRNAi. Scale bars: 20 μm (B and E).

Figure 9A). However, TCPTP-37, at doses that efficiently dephosphorylated GST-pYTβRIICD, failed to dephosphorylate GST-pYTβRIIY284/336/470ACD (Figure 8, D–F), which suggests that Y284, Y336, and/or Y470 in the TβRII cytoplasmic domain are the target tyrosine residues of TCPTP in vitro.

**TβRIIY336 and TβRIIY470 control cell morphology and SMAD activation.** We next defined the relative contribution of TβRIIY284, TβRIIY336, and/or TβRIIY470 in TβR-mediated activation of SMAD-dependent signaling and EMT. To this end,

we crossed α1KO mice with floxed TβRII mice (*Itgal<sup>-/-</sup> Tgfb2<sup>fl/fl</sup>*; referred to herein as α1KO TβRII<sup>fl/fl</sup>), isolated CD cells, and deleted the floxed TβRII alleles using adenoviral Cre (adeno-Cre) infection. The resulting cells were then transfected with human TβRII carrying single or multiple Y-to-A mutations in the TCPTP dephosphorylation sites Y284, Y336, or Y470. While α1KO TβRII<sup>fl/fl</sup> CD cells displayed a fibroblast-like phenotype, adeno-Cre treatment resulted in an epithelial morphology (Figure 9A), similar to α1KO CD cells treated with SB431542 or spermidine (Figure 4A

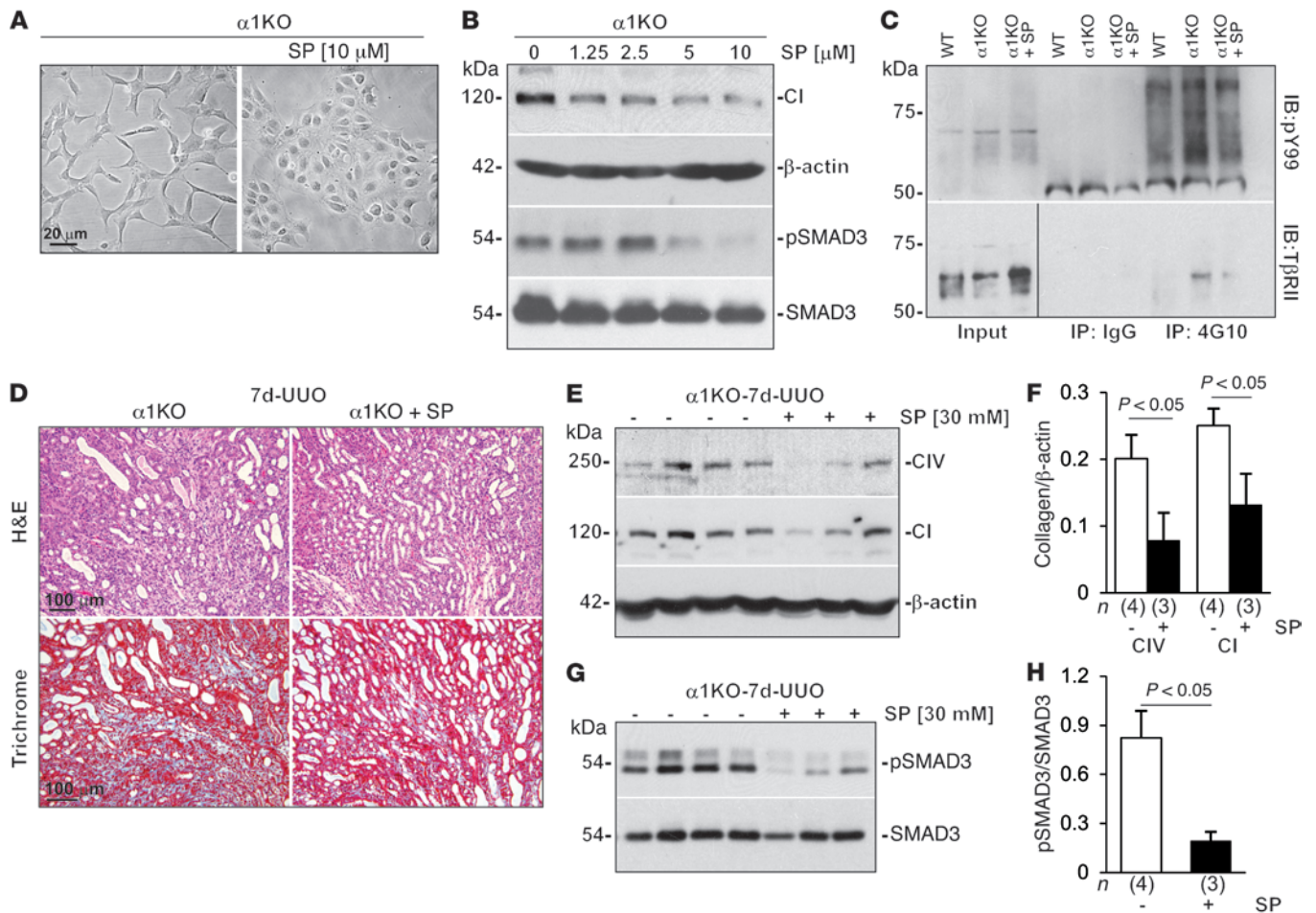


**Figure 7. Spermidine ameliorates TβR-activated signaling in α1KO CD cells and mice.** (A) Morphology of α1KO CD cells cultured on plastic in 0.2% serum with or without spermidine (SP) for 4 days (B) Serum-starved α1KO CD cells were treated with spermidine for 24 hours at the concentrations indicated. Cell lysates (20 μg/lane) were analyzed by Western blot for levels of pSMAD3, SMAD3, and collagen I. (C) Cell lysates (0.5 mg) from serum-starved WT and α1KO CD cells, treated or not for 24 hours with 2.5 μM spermidine, were incubated with 4G10 (10 μg) or mouse IgG isotype control antibody (10 μg). Immunoprecipitation products were then analyzed as in Figure 6A. Lanes were run on the same gel but were noncontiguous (black line). (D) H&E and Trichrome staining of kidneys from α1KO mice untreated or treated with spermidine (30 μM via gavage) at 7 days post-UUO, showing less injury and collagen deposition (blue staining) in the spermidine-treated group. (E and G) Kidney lysates (10 μg/lane) from injured α1KO (n = 4) and spermidine-treated α1KO (n = 3) mice were analyzed by Western blot for levels of collagen I, collagen IV, pSMAD3, and SMAD3. (F and H) Collagen I, collagen IV, β-actin, pSMAD3, and SMAD3 bands were quantified by densitometry analysis; signal is expressed as the collagen I/β-actin or pSMAD3/SMAD3 ratio. Values are mean ± SEM of the indicated n. Scale bars: 20 μm (A); 100 μm (D).

and Figure 7A). As expected, adeno-Cre-treated α1KO TβRII<sup>fl/fl</sup> CD cells transfected with WT TβRII switched to a fibroblast-like phenotype (Figure 9A). Transfection of adeno-Cre-treated α1KO TβRII<sup>fl/fl</sup> CD cells with single-mutant TβRIIY284A, TβRIIY336A, or TβRIIY470A also reverted to a fibroblast-like phenotype, while cells expressing TβRIIY284/336/470A retained the epithelial phenotype (Figure 9A). Interestingly, transfection of adeno-Cre-treated α1KO TβRII<sup>fl/fl</sup> CD cells with TβRII carrying 2 Y-to-A substitutions revealed that only expression of TβRIIY336/470A prohibited the conversion of the epithelial cell morphology to a fibroblast-like phenotype (Figure 9A).

Next, we analyzed subcellular localization of WT TβRII or TβRII carrying single or multiple Y-to-A substitutions fused to EGFP by transiently transfecting expression constructs into HEK293 cells. These constructs localized to the plasma membrane (Figure 9B), excluding aberrant localization of mutant TβRII as a cause for impaired TβRII/TβRI function.

Cell signaling analysis performed on transiently transfected CD cells expressing comparable levels of WT and Y-to-A mutated TβRII revealed that TβRIIY336 and TβRIIY470 controlled SMAD3 activation. CD cells carrying the single TβRIIY336A or TβRIIY470A mutation displayed significantly reduced levels of pSMAD3 compared with cells expressing WT TβRII or TβRIIY284A (Figure 9C and Supplemental Figure 10). Consistent with their epithelial morphology (Figure 9A), only cells expressing the TβRIIY336/470A and TβRIIY284/336/470A mutations showed E-cadherin levels similar to those of adeno-Cre-treated α1KO TβRII<sup>fl/fl</sup> CD cells (Figure 9D and Supplemental Figure 10), which suggests that both Y336 and Y470 are required for regulation of E-cadherin expression. Finally, cells carrying all 3 Y-to-A mutations showed collagen IV levels similar to those of adeno-Cre-treated α1KO TβRII<sup>fl/fl</sup> CD cells (Figure 9D and Supplemental Figure 10), which indicates that TβRII tyrosine phosphorylation-mediated regulation of collagen synthesis is both SMAD dependent and independent.

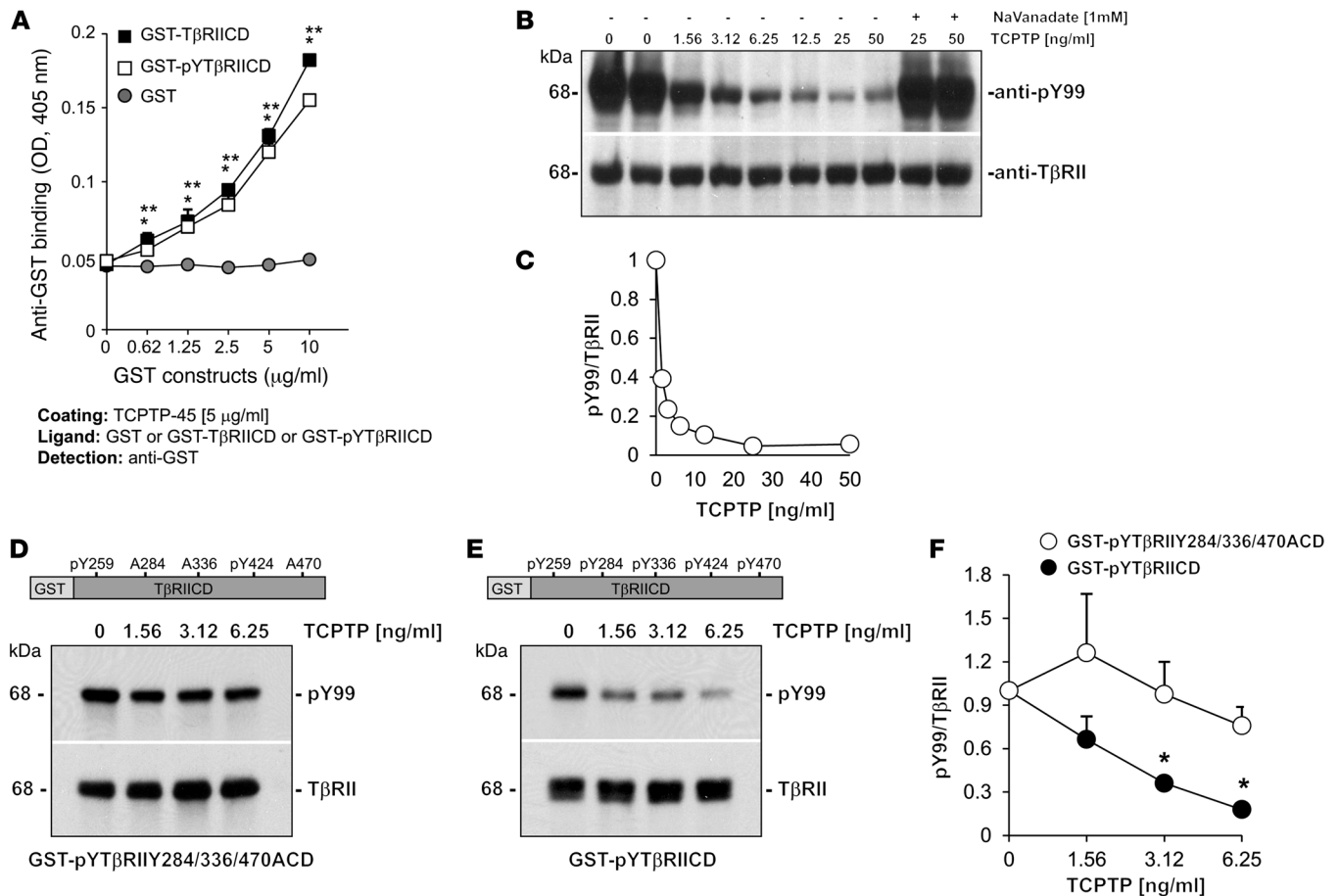


**Figure 8. TCPTP directly binds and dephosphorylates the cytoplasmic tail of T $\beta$ RII.** (A) Immobilized TCPTP (5  $\mu$ g/ml) was incubated with GST, GST-T $\beta$ RIICD, or GST-pYT $\beta$ RIICD at the indicated concentrations. Bound proteins were detected with anti-GST antibodies. Shown is 1 experiment performed in triplicate, representative of 2 independent experiments performed with similar results. Values are mean  $\pm$  SD. \* $P$   $\leq$  0.05 vs. GST-pYT $\beta$ RIICD; \*\* $P$   $\leq$  0.05 vs. GST. (B) GST-pYT $\beta$ RIICD (~50 ng) was incubated with TCPTP-37 at the indicated concentrations, with or without the tyrosine phosphatase inhibitor sodium vanadate. After 10 minutes at 30°C, samples were analyzed by Western blot for levels of phosphorylated (anti-pY99) and total (anti-T $\beta$ RII) GST-pYT $\beta$ RIICD. (C) pY99 and T $\beta$ RII bands were quantified by densitometry. Values represent pY99/T $\beta$ RII ratio relative to samples incubated without TCPTP (assigned as 1). (D and E) GST-pYT $\beta$ RIICD or GST-pYT $\beta$ RIIY284/336/470ACD (~50 ng) was incubated with TCPTP-37 at the indicated concentrations. After 10 minutes at 30°C, samples were analyzed by Western blot for levels of phosphorylated (anti-pY99) and total (anti-T $\beta$ RII) GST-conjugated recombinant proteins. (F) pY99 and T $\beta$ RII bands were quantified by densitometry. Values (mean  $\pm$  SEM of 3 experiments) represent pY99/T $\beta$ RII ratio relative to samples incubated without TCPTP (assigned as 1). \* $P$   $\leq$  0.05 vs. 0 ng/ml.

We next determined the ability of the T $\beta$ RII mutants to activate SMAD3 in response to TGF- $\beta$ 1. For TGF- $\beta$ 1-mediated signaling, we focused on CD cells expressing WT, T $\beta$ RIIY284A (which should promote SMAD3 phosphorylation via Y336 and Y470), and T $\beta$ RIIY284/336/470A (which should not promote SMAD3 activation due to loss of Y336 and Y470). Mock-treated and adeno-Cre-infected  $\alpha$ 1KO T $\beta$ RII<sup>fl/fl</sup> CD cells were used as positive and negative controls, respectively. Western blotting revealed comparable expression levels of WT and Y-to-A mutated T $\beta$ RII. As expected, TGF- $\beta$ 1 promoted SMAD3 activation only in mock-treated  $\alpha$ 1KO T $\beta$ RII<sup>fl/fl</sup> CD cells, or adeno-Cre-treated  $\alpha$ 1KO T $\beta$ RII<sup>fl/fl</sup> CD cells transfected with either WT or T $\beta$ RIIY284A (Figure 9E). In contrast, TGF- $\beta$ 1 failed to stimulate SMAD3 phosphorylation in T $\beta$ RIIY284/336/470A expressing cells (Figure 9E), which suggests that Y336 and Y470 regulate TGF- $\beta$ 1-mediated activation of canonical signaling.

Finally, we sought to determine whether Y284, Y336, and/or Y470 are phosphorylated in  $\alpha$ 1KO CD cells. We immunoprecipitated T $\beta$ RII in cell lysates from adeno-Cre-treated  $\alpha$ 1KO T $\beta$ RII<sup>fl/fl</sup> CD

cells transfected with either WT T $\beta$ RII or T $\beta$ RIIY284/336/470A and immunoblotted the gel-separated precipitates with anti-human T $\beta$ RII or anti-pY99 antibodies, respectively. Adeno-Cre-treated  $\alpha$ 1KO T $\beta$ RII<sup>fl/fl</sup> CD cells served as negative control. Although CD cells expressing WT T $\beta$ RII and T $\beta$ RIIY284/336/470A contained comparable levels of T $\beta$ RII, only cells expressing WT T $\beta$ RII showed substantial T $\beta$ RII tyrosine phosphorylation (Figure 9F). Similarly, reciprocal immunoprecipitation with the anti-phosphotyrosine antibody 4G10 followed by anti-T $\beta$ RII immunoblotting revealed that only CD cells transfected with WT T $\beta$ RII showed tyrosine phosphorylation (Figure 9G). Together, these data confirmed that Y284, Y336, and/or Y470 can be phosphorylated in vivo.

## Discussion

TGF- $\beta$  is widely recognized as one of the key mediators of renal fibrosis, which eventually leads to chronic kidney disease. Its role in this pathological process has primarily been investigated in the context of increased or activated signaling. However, pathways

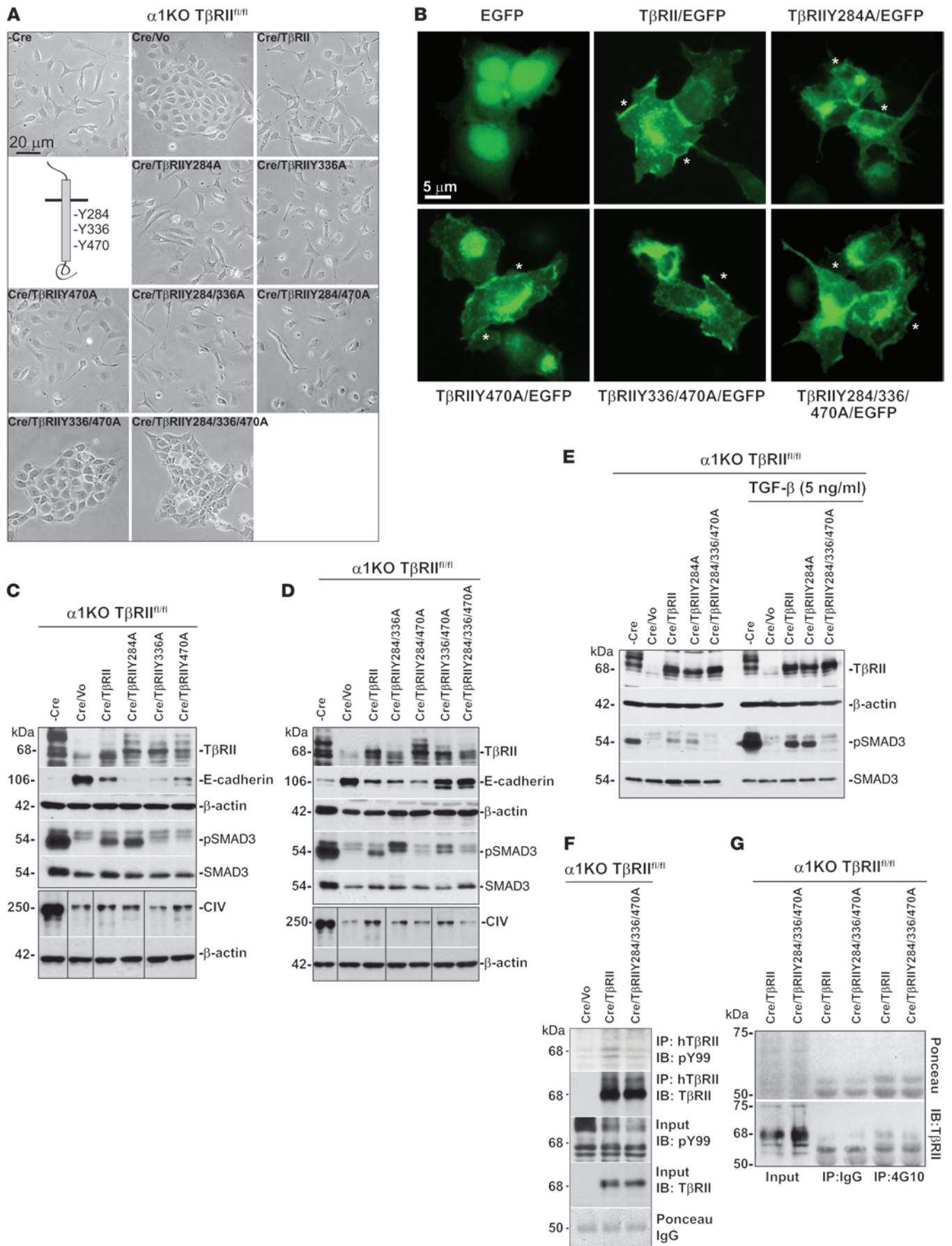


**Figure 9. Y336 and Y470 in the cytoplasmic tail of T $\beta$ RII regulate EMT.**

(A)  $\alpha$ 1KO T $\beta$ RII<sup>fl/fl</sup> CD cells were left untreated (-Cre) or treated with adeno-Cre (Cre) to downregulate T $\beta$ RII. Cells were then transfected with empty vector (Cre/Vo), WT T $\beta$ RII (Cre/T $\beta$ RII), or T $\beta$ RII constructs mutated in 1 or more of the 3 tyrosines (as indicated), and their morphology was evaluated. (B) HEK293 cells were transiently transfected with empty pEGFP-N2 vector (EGFP), WT T $\beta$ RII (T $\beta$ RII/EGFP), or T $\beta$ RII constructs mutated in 1 (T $\beta$ RIIY284A/EGFP and T $\beta$ RIIY470A/EGFP) or multiple (T $\beta$ RIIY336/470A/EGFP and T $\beta$ RIIY284/336/470A/EGFP) tyrosines. After 72 hours, the membrane localization (asterisks) of the various T $\beta$ RII constructs was evaluated by analyzing the cells under an epifluorescence microscope. (C and D) Cell lysates (20  $\mu$ g/lane) from the serum-starved CD cell populations indicated were analyzed by Western blot for levels of T $\beta$ RII, pSMAD3, SMAD3, collagen IV, and E-cadherin. Lanes were run on the same gel but were noncontiguous (black lines). (E) The indicated CD cell populations were serum starved for 24 hours, then treated or not with TGF- $\beta$ 1 for 30 minutes. Cell lysates (20  $\mu$ g/lane) were analyzed by Western blot for levels of T $\beta$ RII, pSMAD3, and SMAD3. (F and G) Cell lysates (0.5 mg) from the serum-starved CD cell populations indicated were immunoprecipitated with anti-human T $\beta$ RII antibodies (2  $\mu$ g) (F) or with 4C10 (10  $\mu$ g) or mouse IgG isotype control antibody (10  $\mu$ g) (G), then analyzed by Western blot. A band corresponding to T $\beta$ RII was more tyrosine phosphorylated (F) and more evident (G) in lysates of CD cells expressing WT than Y284/336/470A T $\beta$ RII. Scale bars: 20  $\mu$ m (A); 5  $\mu$ m (B).

and mechanisms that inhibit or negatively modulate TGF- $\beta$  signaling are equally important, particularly in the context of limiting fibrotic responses and scarring after injury. In the present study, we report the novel finding that T $\beta$ RII-mediated profibrotic signaling in a kidney model of tubulointerstitial fibrosis can be downregulated by decreasing T $\beta$ RII tyrosine phosphorylation in an integrin  $\alpha$ 1 $\beta$ 1-dependent manner (Figure 10). Our data suggest that targeting T $\beta$ RII tyrosine phosphorylation may represent an innovative strategy by which to attenuate renal fibrosis.

Here, we showed that loss of integrin  $\alpha$ 1 $\beta$ 1 led to increased TGF- $\beta$ -mediated signaling and fibrosis upon UUO. This, together with the observations of increased SMAD2 and SMAD3 activation in mice and cells lacking integrin  $\alpha$ 1 $\beta$ 1, suggests that activation of TGF- $\beta$ -mediated canonical signaling is a major driver of tubular kidney fibrosis in mice null for integrin  $\alpha$ 1. Our observations were consistent with findings by others demonstrating upregulated levels of TGF- $\beta$ , its receptors, and pSMAD2 and pSMAD3 in many types of chronic kidney disease (17, 38). SMAD2 can promote fibrosis by promoting  $\alpha$ SMA and collagen expression (39, 40). SMAD3 induces fibrosis by upregulating the profibrotic miR-21 and collagen synthesis (40, 41). Thus, strategies for decreasing T $\beta$ R-mediated activation of SMAD2 and SMAD3 might effectively dampen TGF- $\beta$ -induced fibrotic signaling.

We previously showed that in vivo deletion of T $\beta$ RII in CDs of the kidney leads to an exacerbated UUO-mediated fibrotic response (42). Absence of T $\beta$ RII in CD cells caused cytoskeletal changes and alterations in Rho GTPases that resulted in increased TGF- $\beta$  activation and paracrine activation of profibrotic signaling. In our current study, we showed that upregulated basal activation of T $\beta$ RII in CDs and CD cells also contributed to fibrotic responses by increasing epithelial SMAD3 activation, EMT, and collagen synthesis. Thus, upregulation of T $\beta$ R signaling in nonepithelial (42) and epithelial (present study) cells makes a contribution to kidney fibrosis. Although we provided evidence that blocking

T $\beta$ R signaling in  $\alpha$ 1KO CD cells reduced profibrotic signaling, it remains to be evaluated whether in vivo deletion and/or inhibition of T $\beta$ RII in CDs of  $\alpha$ 1KO mice ameliorates or exacerbates UUO-mediated fibrosis due to compensation by the remaining tubules or nonepithelial components.

T $\beta$ R1 and T $\beta$ R2 are serine/threonine kinases that phosphorylate SMAD2 and SMAD3 to trigger fibrosis. The majority of studies thus far focused on serine phosphatases acting on either the T $\beta$ R complex and/or SMADs as potential attenuators of TGF- $\beta$  signaling (43). The catalytic subunit of PP1 (PP1c), for example, dephosphorylates T $\beta$ R1 and ameliorates TGF- $\beta$ -mediated EMT (44, 45); PP2A dephosphorylates SMAD3 primarily under hypoxic conditions (46), MTMR4 dephosphorylates SMAD3 in early endosomes and thereby prevents SMAD3 nuclear translocation (47), and PPM1A can dephosphorylate both SMAD2 and SMAD3 (48). We provided compelling evidence that tyrosine phosphatases play an equally important role as negative regulators of TGF- $\beta$ -mediated signaling by directly controlling the levels of tyrosine phosphorylation of the T $\beta$ RII cytoplasmic domain.

The T $\beta$ RII cytoplasmic tail is primarily phosphorylated on serines. Autophosphorylation of S213 and S409 is necessary for kinase activity and interaction with T $\beta$ R1, whereas autophosphorylation of S416 inhibits the receptor activity of T $\beta$ R2 (5). It has also been shown that T $\beta$ RII is phosphorylated on different tyrosine residues. One report suggested that T $\beta$ RII undergoes autophosphorylation on tyrosines Y259, Y336, and Y424, while another showed that activated Src is able to phosphorylate Y284 (6, 7). Mutations of Y259, Y336, and Y424 inhibit the receptor kinase activity of T $\beta$ RII (6), while mutation of Y284 prevents T $\beta$ R-mediated activation of the noncanonical p38 MAPK signaling pathway (7). We demonstrated here that Y336 and Y470 were key mediators of T $\beta$ RII-mediated EMT, SMAD activation, and E-cadherin and collagen synthesis. While we identified these tyrosines as critical regulators of T $\beta$ RII-mediated SMAD activation and fibrotic responses, it remains to be determined exactly how Y336 and Y470 become phosphorylated, although autophosphorylation and Src are possible candidates (6, 7).

Another key finding of our present study is that the levels of tyrosine phosphorylation of the T $\beta$ RII cytoplasmic tail were negatively regulated by TCPTP. Of the 5 phosphorylatable tyrosines in the T $\beta$ RII cytoplasmic tail, we identified 3 of them (Y284, Y336, and Y470) as potential TCPTP dephosphorylation substrates. TCPTP, a tyrosine phosphatase initially discovered in T cells, is ubiquitously expressed and localizes to the nucleus and endoplasmic reticulum (49). The nuclear form translocates to the cytoplasm in response to growth factor receptor activation, cellular stress, and oxidative stress (50). Normally, TCPTP remains in an autoinhibitory state by an association between the C-terminal segment and the phosphatase domain. TCPTP can directly bind the cytoplasmic tail of the integrin  $\alpha$ 1 subunit, which enables TCPTP recruitment to the plasma membrane and activation via an integrin  $\alpha$ 1-mediated unbinding of the C-terminal segment from the catalytic domain (31). We and others have shown that integrin  $\alpha$ 1 $\beta$ 1-mediated TCPTP activation induces the dephosphorylation of TCPTP substrates, including receptors for EGF, VEGF, and PDGF, resulting in downregulation of their signaling strength (25, 31–33). We report here that the integrin  $\alpha$ 1 $\beta$ 1/TCPTP axis also plays a key

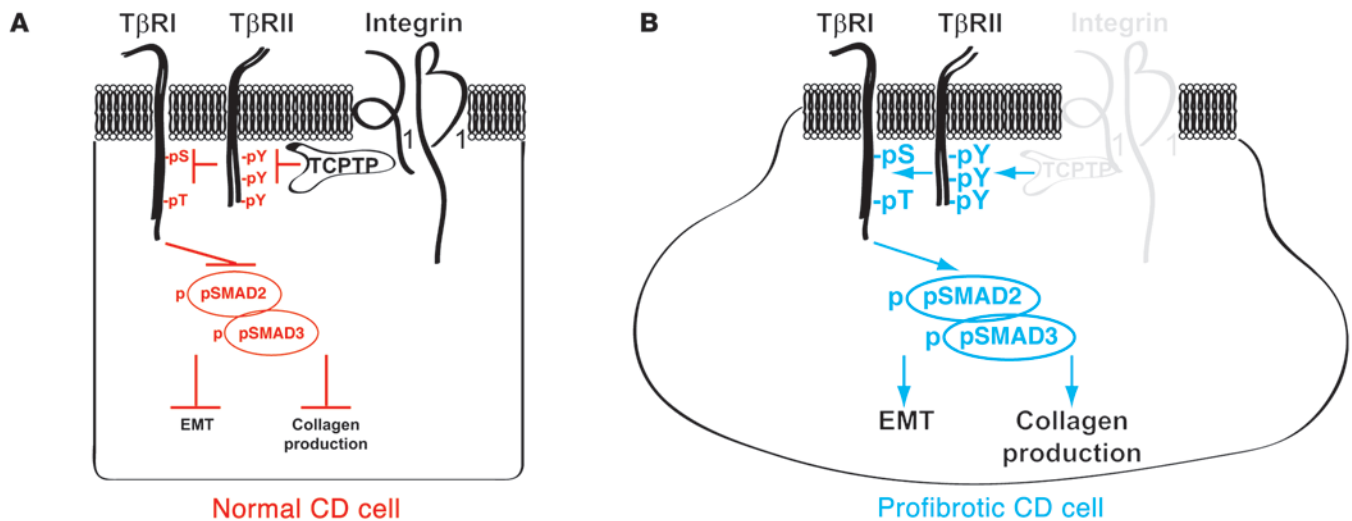


**Figure 10. Integrin  $\alpha 1\beta 1$  controls T $\beta$ RII-mediated cell morphology and collagen production. (A)** In CD cells, activation of integrin  $\alpha 1\beta 1$  leads to recruitment and activation of TCPTP. This results in reduced tyrosine phosphorylation of T $\beta$ RII, reduced activation of T $\beta$ RI, and reduced SMAD2/3 phosphorylation. Ultimately, recruitment of TCPTP by integrin  $\alpha 1\beta 1$  negatively regulates T $\beta$ RI/T $\beta$ RII-mediated collagen production and EMT. **(B)** In the absence of integrin  $\alpha 1\beta 1$ , loss of TCPTP activation promotes collagen production and EMT by increasing tyrosine phosphorylation of T $\beta$ RII, activation of T $\beta$ RI, and SMAD2/SMAD3 phosphorylation.

role in negatively regulating the T $\beta$ RII tyrosine phosphorylation, as loss of integrin  $\alpha 1\beta 1$  expression or TCPTP function led to tyrosine hyperphosphorylation of T $\beta$ RII, activation of T $\beta$ RI, phosphorylation of SMAD2/3, and expression of fibrotic genes, culminating in irreversible tissue damage. Thus, we identified T $\beta$ RII as a novel *in vivo* target of TCPTP and suggest that strategies for enhancing TCPTP activation might be beneficial in fibrotic disease.

Due to the ability of TCPTP to dephosphorylate growth factor receptors implicated in several diseases, including cancer, TCPTP activation became an attractive strategy to prevent receptor tyrosine kinase-mediated signaling. High-throughput small-molecule assays identified the polyamine spermidine as a TCPTP activator (33). Like the integrin  $\alpha 1$  tail, spermidine triggers unbinding of the C-terminal segment of TCPTP, which in turn attenuates tyrosine receptor kinase phosphorylation (33). We also found that treatment of CD cells or mice lacking integrin  $\alpha 1\beta 1$  with spermidine decreased T $\beta$ RII tyrosine dephosphorylation, T $\beta$ R-mediated SMAD activation, and profibrotic signaling. Although our findings suggest that activation of TCPTP might be beneficial in TGF- $\beta$ -driven fibrotic diseases, spermidine is not a selective TCPTP activator. It has previously been shown that long-term polyamine intake can have both beneficial and deleterious effects: it can decrease mortality and incidence of colon cancer in aged mice (51) and protect against cardiovascular mortality in humans (52), but can also cause a decline in human renal function (53). Nevertheless, our findings support the need to generate more selective and safer TCPTP activators for the prevention and treatment of TGF- $\beta$ -mediated kidney disease.

## Methods

**Mice.**  $\alpha 1$ KO mice (*Itga1*<sup>-/-</sup>; global integrin  $\alpha 1$ -null) were generated as previously described (54). Inbred BALB/c  $\alpha 1$ KO mice were generated by backcrossing the  $\alpha 1$ KO mice onto the WT BALB/c background. After 10 generations, integrin  $\alpha 1$ -heterozygous siblings were crossed among themselves in order to obtain BALB/c WT and  $\alpha 1$ KO mice.

T $\beta$ RII<sup>fl/fl</sup> mice backcrossed onto the C57BL/6 background for 10 generations were derived as described previously (42). These mice were crossed with BALB/c  $\alpha 1$ KO mice in order to obtain F1 integrin  $\alpha 1$ -heterozygous T $\beta$ RII<sup>fl/+</sup> mice on the mixed C57/BALB/c background. These mice were crossed among themselves in order to obtain  $\alpha 1$ KO T $\beta$ RII<sup>fl/fl</sup> mice. Mice were housed in an AALAC-accredited animal facility following NIH guidelines.

**Generation of cell populations.** CD cells were generated from BALB/c WT and  $\alpha 1$ KO mice as well as from  $\alpha 1$ KO T $\beta$ RII<sup>fl/fl</sup> mice on the mixed C57/BALB/c background. Briefly, papillae were dissected from kidneys, placed in 1 mg/ml collagenase II (Gibco) with 5 mM CaCl<sub>2</sub>, minced with a razor blade, and incubated for 1 hour at 37°C. Cells were centrifuged for 3 minutes at 800 *g* and washed twice with PBS before plating. Cells were cultured in DMEM/F12 supplemented with 10% FBS and immortalized with sv40 large T antigen. T $\beta$ RII was deleted from  $\alpha 1$ KO T $\beta$ RII<sup>fl/fl</sup> CD cells by adeno-Cre infection. Unless otherwise specified, cells used for experiments were cultured on uncoated tissue culture plates in either complete or serum-free medium.

**Cell transfection.**  $\alpha 1$ KO-Rec CD cells were obtained by transfecting  $\alpha 1$ KO CD cells (derived from BALB/c mice) with the full-length human integrin  $\alpha 1$  subunit cDNA subcloned in pcDNA3.1 vector (Invitrogen) (55). After selection with zeocin (200  $\mu$ g/ml), integrin  $\alpha 1$ -expressing cells were selected by fluorescence-activated cell sorting using antibodies recognizing the extracellular I domain of human integrin  $\alpha 1$  subunit (TS2/7) (Abcam).

To generate cell populations expressing WT or Y-to-A mutants of human T $\beta$ RII,  $\alpha 1$ KO T $\beta$ RII<sup>fl/fl</sup> CD cells (derived from the C57/BALB/c mixed background) were treated with adeno-Cre in order to delete endogenous T $\beta$ RII. Subsequently, adeno-Cre-treated cells were transfected with pcDNA3.1 vector carrying full-length WT human T $\beta$ RII, as well as single, double, or triple Y-to-A (Y284A, Y336A, Y470A) mutants of human T $\beta$ RII using Lipofectamine 2000 (Invitrogen). The Y-to-A mutations were introduced in full-length T $\beta$ RII using QuickChange II XL Site-Directed Mutagenesis Kit (Agilent Technologies). After zeocin selection (200  $\mu$ g/ml),

levels of T $\beta$ RII were analyzed by Western blot. In some experiments, transient transfections were performed, and T $\beta$ RII levels were analyzed 72–96 hours after transfection. Primers and PCR conditions used for the generation of the T $\beta$ RII constructs are summarized below.

To downregulate TCPTP expression, WT CD cells were transfected with pLKO.1-puro vector carrying TCPTP-targeted shRNAi (TRCN000029889; Sigma-Aldrich) or nontargeted shRNAi control (SHC002; Sigma-Aldrich) using Infecting Transfection Reagent (QIAGEN). After selection with puromycin (1  $\mu$ g/ml), single clones were isolated and analyzed by Western blot for TCPTP levels.

To generate T $\beta$ RII constructs fused to EGFP, WT or Y-to-A mutated T $\beta$ RII DNA constructs were subcloned into pEGFP-N2 plasmid (Clontech) using the primers and PCR conditions summarized below. Human HEK293 cells (CRL-1573; ATCC) were subsequently transfected with these constructs or empty vector using Lipofectamine 2000 (Invitrogen). After 72 hours, cells were fixed with 4% paraformaldehyde in PBS, and the localization of the T $\beta$ RII-EGFP constructs was analyzed by placing the cells under an epifluorescence microscope (Nikon).

**Recombinant proteins.** The full-length recombinant TCPTP (TCPTP-45) carrying an N-terminal His6 tag was prepared as previously described (24). To generate GST-human T $\beta$ RII constructs carrying the sequence of the C-terminal 374 amino acids (R193–K567) of T $\beta$ RII (GST-T $\beta$ RIICD; Supplemental Figure 9A), the primers and conditions described below were used. The PCR product was subcloned into pGEX6p, and the plasmid was then transformed in BL21 (Novagen) competent *E. coli*. GST-T $\beta$ RIICD constructs were purified from isopropyl  $\beta$ -D-thiogalactoside-induced bacterial lysates using glutathione-agarose (Sigma-Aldrich), as described previously (24). Purified protein was analyzed by SDS-PAGE and Western blot using antibodies against the cytoplasmic domain of T $\beta$ RII (Santa Cruz) (Supplemental Figure 9B). To generate phosphorylated WT and Y-to-A mutated T $\beta$ RIICD constructs, the pGEX6p encoding GST-T $\beta$ RIICD or GST-T $\beta$ RIIY284/336/470ACD constructs were transformed in TKB1 competent *E. coli* (Stratagene), as described previously (24). This strain is a derivative of the BL21 strain, with the exception that it harbors a plasmid encoding a tyrosine kinase gene inducible by the addition of indoleacrylic acid (10  $\mu$ g/ml). Tyrosine-phosphorylated GST-pYT $\beta$ RIICD constructs were analyzed by SDS-PAGE and Western blot using anti-T $\beta$ RII and anti-pY99 antibodies (Santa Cruz) (Supplemental Figure 9C).

**Generation of human T $\beta$ RII full-length or mutant constructs.** For generation of T $\beta$ RII constructs subcloned in pCDNA3.1zeo, the following primers carrying *HindIII* and *EcoRI* restriction sites were generated: T $\beta$ RII, 5'-ATATAAGCTTGCCACCATGATGGGTCTGGGGGCTGCTC and 3'-ATATGAATTCTACTACTATTTGGTAGTGTTTACCCAC; T $\beta$ RII/Y284A, 5'-AAGATCTTCCCTATGAGGAGGCCGCTCTT-GGAAGACAGAGAAG and 3'-CTTCTGTCTTCCAAGAGGCG-GCCTCCTCATAGGAAAGATCTT; T $\beta$ RII/Y336A, 5'-GGCAACCTACAGGAGGCCCTGACGCGGCATGT and 3'-ACATGCCGCGTCAGGGCCCTCTGTAGGTTGCC; T $\beta$ RII/Y470A, 5'-GTAATGCAAGTGGGAGAAGTAAAGATGCTGAGCCTCCATTTGG and 3'-CCAAATGGAGGCTCAGCATCTTTACTTCTCCACTGCAT-TAC. PCR conditions were as follows: 1 cycle of 95°C for 45 seconds; 30 cycles of 95°C for 45 seconds, 63°C for 45 seconds, and 72°C for 2 minutes; and 1 cycle of 72°C for 10 seconds.

To generate T $\beta$ RII cytoplasmic domain in pGEX6p, the following primers carrying *EcoRI* and *XhoI* restriction sites were generated: T $\beta$ RIICD(R193–K567), 5'-ATATGAATTCCGGCAGCAGAAGCTGA-

GTTC and 3'-ATATCTCGAGCTACTACTATTTGGTAGTGTTTAG-GGAG. PCR conditions were as follows: 1 cycle of 95°C for 45 seconds; 30 cycles of 95°C for 45 seconds, 63°C for 45 seconds, and 72°C for 2 minutes; and 1 cycle of 72°C for 10 seconds.

To generate T $\beta$ RII WT or mutant constructs in pEGFP-N2, the following common primers carrying *HindIII* and *BamHI* restriction sites were generated: 5'-ATATAAGCTTGCCACCATGGGTCTGGGGGCT-GC and 3'-ATATGGATCCCTTTGGTAGTGTTTAGGGAG. PCR conditions were as follows: 1 cycle of 95°C for 45 seconds; 30 cycles of 95°C for 45 seconds, 52°C for 45 seconds, and 72°C for 2.5 minutes; and 1 cycle of 72°C for 10 seconds.

**Immunoprecipitation.**  $\alpha$ 1KO-Rec CD cells expressing the human integrin  $\alpha$ 1 subunit were lysed in lysis buffer (1% CHAPS, 50 mM Tris, pH 7.5, containing 150 mM NaCl, 2 mM MgCl<sub>2</sub>, 5 mM iodoacetamide, and protease inhibitors; Roche Applied Science), spun at 16,000 *g* for 20 minutes, and preincubated with BSA-blocked protein G beads for 1 hour at 4°C. Equal amounts of cell lysates (0.5 mg) were subsequently incubated overnight at 4°C with either monoclonal antibody TS2/7 (20  $\mu$ g) or mouse IgG1 isotype control antibody (20  $\mu$ g; Millipore). The antibody-antigen complexes were captured with BSA-blocked protein G-agarose beads for 1 hour at 4°C, washed with wash buffer (50 mM Tris, pH 7.5, containing 150 mM NaCl, and 0.1% Tween 20), eluted in sample buffer, resolved by SDS-PAGE in 10% gels under reducing conditions, and analyzed by Western blot with antibodies against the human integrin  $\alpha$ 1 subunit T $\beta$ RII (TS2/7; Santa Cruz) and TCPTP (R&D Systems).

To detect murine tyrosine-phosphorylated T $\beta$ RII, equal amounts of cell lysates (0.5 mg) were precleaned as described above and subsequently incubated overnight at 4°C with either the anti-phosphotyrosine antibody 4G10 (10  $\mu$ g; Millipore) or IgG2b isotype control antibody (10  $\mu$ g; Millipore). The antibody-antigen complexes, captured and resolved by SDS-PAGE as described above, were detected by Western blot using anti-pY99 and/or anti-T $\beta$ RII antibodies.

To detect human phosphorylated T $\beta$ RII, equal amounts of cell lysates (0.5 mg) from CD cells expressing human WT T $\beta$ RII or T $\beta$ RIIY284/336/470A were precleaned as described above and subsequently incubated overnight at 4°C with anti-human T $\beta$ RII antibody (2  $\mu$ g; R&D Systems; ref. 56). The antibody-antigen complexes, captured and resolved by SDS-PAGE as described above, were detected by Western blot using anti-pY99 and anti-T $\beta$ RII antibodies.

To detect mouse pT $\beta$ R1, CD cells were lysates as described above. Equal amounts of cell lysates (0.5 mg) were precleaned as described above and subsequently passed through columns conjugated to phosphoserine and phosphothreonine antibodies according to the manufacturer's instructions (QIAGEN). The antibody-antigen complexes, captured and resolved by SDS-PAGE as described above, were detected by Western blot using anti-phosphoserine (Millipore) or anti-T $\beta$ R1 antibodies (Abcam).

**In vitro T $\beta$ RII tyrosine dephosphorylation assay.** GST-pYT $\beta$ RIICD recombinant proteins (~50 ng) were incubated with commercially available constitutively active TCPTP (TCPTP-37; 0–50 ng/ml; R&D Systems) in 100 mM Tris, pH 7.5, containing 20 mM DTT, 2 mM EDTA, 1 mM EGTA, 5 mg/ml BSA, 0.1% Brij 35, and protease inhibitors with or without the tyrosine phosphatase inhibitor sodium vanadate (1 mM). After 10 minutes at 30°C, the samples were separated in SDS-PAGE, transferred to nitrocellulose, and probed with anti-pY99 or anti-T $\beta$ RII antibodies.

**Solid-phase ligand binding assays.** To determine GST-T $\beta$ RRIICD binding to TCPTP, plates were coated at 4°C with purified His-TCPTP-45 at 5  $\mu$ g/ml in 50 mM sodium bicarbonate buffer, pH 9.5. After 24 hours, plates were treated with 5 mM iodoacetamide for 30 minutes at room temperature, then blocked with 0.5% BSA in 50 mM Tris, pH 7.5, containing 150 mM NaCl. GST, GST-T $\beta$ RRII, or GST-pYT $\beta$ RRII, at various concentrations in 50 mM Tris, pH 7.5, containing 150 mM NaCl, 0.1% BSA, and 0.1% Tween 20, were added to the wells and incubated overnight at 4°C. After extensive washing (50 mM Tris, pH 7.5, containing 150 mM NaCl and 0.1% Tween), bound proteins were detected with anti-GST antibody (Cell Signaling), followed by appropriate HRP-conjugated secondary antibody. HRP substrate (Bio-Rad) was added to the wells, and absorbance was monitored at 650 nm. BSA-coated wells were used as controls for nonspecific binding.

**Flow cytometry.** To determine integrin expression levels, CD cells were incubated with anti-mouse integrin  $\alpha$ 1,  $\alpha$ 2,  $\alpha$ 5,  $\alpha$ v,  $\beta$ 1,  $\beta$ 3 (BD Biosciences), or  $\alpha$ v $\beta$ 6 (Chemicon) antibodies or with anti-human integrin  $\alpha$ 1 (TS2/7; Abcam) for 1 hour at room temperature, washed, incubated with appropriate phycoerythrin-conjugated secondary antibodies, and analyzed with FACScan (BD Biosciences). Data collected in flow cytometry experiments were analyzed using Cell Quest software (BD Biosciences).

**UUO kidney model.** Only 6- to 8-week-old male WT and  $\alpha$ 1KO BALB/C mice were used for analysis. Mice were randomly divided into control (sham) or experimental (UUO) groups. Surgery was performed by exposing the right kidney through a flank incision and then immediately closing the incision (sham) or ligating the ureter just distal to the renal pelvis (UUO). In some experiments,  $\alpha$ 1KO mice were randomly divided into groups receiving spermidine (150 mM in water, 10  $\mu$ l/g body weight, daily) or water control via gavage starting at the time of UUO. All mice were sacrificed 7 days after surgery.

**Kidney immunohistochemistry and immunofluorescence.** Mouse kidney paraffin sections were incubated with FITC-conjugated dolichos biflorus agglutinin (DBA; Vector Laboratories), anti-collagen I (MD Biosciences), or anti-pSMAD3 (Rockland Immunochemical Inc.) antibodies followed by the appropriate RITC-conjugated secondary antibodies (Calbiochem). Some slides were incubated with anti-F4/80 antibodies (1:100; eBioscience), followed by the appropriate HRP-conjugated secondary antibody and Sigma Fast DAB chromogenic tablets (Sigma-Aldrich). H&E and Trichrome staining were performed according to the kit's instructions (Sigma-Aldrich). Slides were analyzed in a blind fashion under an epifluorescence or light microscope (Nikon).

Human kidney frozen sections (5  $\mu$ m) were incubated with RITC-conjugated DBA (Vector Laboratories) together with mouse anti-human integrin  $\alpha$ 1 (TS2/7; Abcam), rabbit anti-T $\beta$ RRII (Santa Cruz), or mouse anti-TCPTP (Millipore) antibodies followed by the appropriate FITC-conjugated secondary antibodies (Calbiochem). Some slides were incubated with anti-human integrin  $\alpha$ 1 together with anti-T $\beta$ RRII, or anti-T $\beta$ RRII together with anti-TCPTP, to visualize colocalization of these proteins within kidneys. Slides were analyzed under an epifluorescence microscope (Nikon).

**Immunofluorescence.** To visualize ZO-1 and  $\alpha$ SMA, CD cells were plated in 1% fetal calf serum on chamber slides in the presence or absence of SB431542 (10  $\mu$ M; Tocris Bioscience) or the TCPTP inhibitor compound 8 (10 nM) (34). After 3–4 days, cells were fixed in 4% formaldehyde for 10 minutes and permeabilized with 0.1% Triton X-100 in PBS for 5 minutes. After blocking with 3% BSA in PBS, cells were incubated with anti-ZO-1 (Invitrogen) or anti- $\alpha$ SMA (Invitrogen)

antibodies, followed by the appropriate RITC- or FITC-conjugated secondary antibodies (Calbiochem). Slides were mounted with anti-fade mounting medium (VECTASTAIN; Vector Labs) and analyzed in a blind fashion under an epifluorescence microscope (Nikon).

**Measurement of total and active TGF- $\beta$ .** Proteins were extracted from medullary and inner cortical regions of kidneys 7 days after UUO in a detergent-free lysis buffer (50 mM Tris, pH 7.4, containing 150 mM NaCl and protease and phosphatase inhibitors). 72-hour serum-free conditioned medium was collected from WT and  $\alpha$ 1KO CD cells. Latent TGF- $\beta$  in tissue and medium was activated by acidification, allowing for quantification of total TGF- $\beta$  using the Quantikine TGF- $\beta$ 1 ELISA kit (R&D Systems). Equivalent amounts of protein were used, and values were reported as either pg/mg or pg/ $\mu$ g protein. Bioactive TGF- $\beta$  was determined by incubating the tissue lysates or conditioned medium with mink lung epithelial cells containing a TGF- $\beta$ -responsive element in the PAI/L, as described previously (57).

**Alteration of TGF- $\beta$  signaling.** Serum-starved WT and  $\alpha$ 1KO CD cells were treated with the anti-TGF- $\beta$  antibody 2G7 (0–40  $\mu$ g/ml; gift from R. Mernaugh, Vanderbilt University, Nashville, Tennessee, USA) in serum-free medium. After 24 hours, cells were lysed as described above, and levels of pSMAD3 and total SMAD3 were analyzed by Western blot. To confirm the ability of 2G7 to block TGF- $\beta$ -dependent SMAD3 activation, WT CD cells, incubated with or without 2G7, were treated with TGF- $\beta$  (5 ng/ml; R&D Systems) 1 hour prior to harvesting.

To determine the ability of WT and  $\alpha$ 1KO CD cells to respond to TGF- $\beta$ 1, serum-starved CD cells were treated with TGF- $\beta$ 1 (5 ng/ml) for 0–6 hours. Cells were then lysed as described above, and levels of pSMAD3 and total SMAD3 were analyzed by Western blot.

**Densitometry analysis of Western blots.** To quantify levels of collagen or pSMAD in CD cells or tissues, immunoreactive bands were quantified by densitometry analysis, and collagen and pSMAD signals were expressed as collagen/ $\beta$ -actin and pSMAD/SMAD ratios, respectively (values represent AU). To quantify the degree of TCPTP-mediated dephosphorylation of GST-pYT $\beta$ RRII recombinant proteins, pY99 and T $\beta$ RRII immunoreactive bands were quantified as described above, and pY99 signal was expressed as the pY99/T $\beta$ RRII ratio (values represent fold change relative to samples incubated in the absence of TCPTP).

**Western blots.** Proteins from obstructed kidney tissue were extracted using lysis buffer (50 mM Tris HCl, pH 7.4, containing 150 mM NaCl, 1 mM EDTA, 2% SDS, 1% TritonX-100, phosphatase inhibitors, and protease inhibitor cocktail) and homogenized by sonication. Lysates were clarified by centrifugation, and equal amounts of total protein were separated onto SDS-PAGE and subsequently transferred to nitrocellulose membranes. Membranes were blocked in 5% milk and then incubated with various primary antibodies followed by the appropriate HRP-conjugated secondary antibodies. Immunoreactive bands were identified using enhanced chemiluminescence according to the manufacturer's instructions and quantified by densitometry.

CD cells were cultured in serum-free medium with or without SB431542 (0–10  $\mu$ M), spermidine (0–2.5  $\mu$ M), or the TCPTP inhibitor compound 8 (0–10 nM). After 24 hours, proteins were extracted using RIPA buffer (50 mM Tris, pH 7.2, containing 150 mM NaCl, 0.1% SDS, 0.5% sodium deoxycholate, 1% NP40, proteinase inhibitor cocktails, and 4 mM sodium vanadate) Equal amounts of cell lysates were analyzed as described above. Primary antibodies included collagen I (MD Biosciences), collagen IV (BioDesign), pSMAD2 (Cell Signaling), pSMAD3 (Cell Signaling), total SMAD2 (Cell Signaling), total SMAD3

(Cell Signaling),  $\beta$ -actin (Santa Cruz),  $\alpha$ SMA (Sigma-Aldrich), E-cadherin (BD Bioscience), aquaporin-2 (Alpha-Diagnostics), ZEB1 (Santa Cruz), T $\beta$ RI (Abcam), and T $\beta$ RII (Santa Cruz).

**Statistics.** Unpaired, 2-tailed Student's *t* test was used for analysis of 2 independent groups. 1-way ANOVA followed by Tukey HSD test for post-ANOVA pairwise comparisons was used for analysis of multiple groups. A *P* value of 0.05 or less was considered significant.

**Study approval.** All animal experiments were performed in accordance with the guidelines of the Vanderbilt University IACUC.

## Acknowledgments

This work was in part supported by Veterans Affairs Merit Reviews 1I01BX002025-01 (to A. Pozzi) and 1I01BX002196-01 (to R. Zent);

a Veterans Affairs Career Development Award (to L. Gewin); NIH grants DK095761 (to A. Pozzi), DK075594 (to R. Zent), DK069221 (to R. Zent), DK083187 (to R. Zent), DK65123 (to R. Zent and A. Pozzi), and DK099467 (to R.M. Vanacore); and an American Heart Association Established Investigator Award (to R. Zent). This material is the result of work supported with resources at the VA Tennessee Valley Healthcare System.

Address correspondence to: Xiwu Chen or Ambra Pozzi, Division of Nephrology and Hypertension, Medical Center North, B3115, Vanderbilt University, Nashville, Tennessee 37232, USA. Phone: 615.322.4635; E-mail: xiwu.chen@vanderbilt.edu (X. Chen). Phone: 615.322.4637; E-mail: ambra.pozzi@vanderbilt.edu (A. Pozzi).

- Pozzi A, Voziyan PA, Hudson BG, Zent R. Regulation of matrix synthesis, remodeling and accumulation in glomerulosclerosis. *Curr Pharm Des.* 2009;15(12):1318-1333.
- Pozzi A1, Zent R. Integrins in kidney disease. *J Am Soc Nephrol.* 2013;24(7):1034-1039.
- Xu P, Liu J, Derynck R. Post-translational regulation of TGF-beta receptor and Smad signaling. *FEBS Lett.* 2012;586(14):1871-1884.
- Massague J, Xi Q. TGF- $\beta$  control of stem cell differentiation genes. *FEBS Lett.* 2012;586(14):1953-1958.
- Luo K, Lodish HF. Positive and negative regulation of type II TGF- $\beta$  receptor signal transduction by autophosphorylation on multiple serine residues. *EMBO J.* 1997;16(8):1970-1981.
- Lawler S, et al. The type II transforming growth factor- $\beta$  receptor autophosphorylates not only on serine and threonine but also on tyrosine residues. *J Biol Chem.* 1997;272(23):14850-14859.
- Gallagher AJ, Schiemann WP. Src phosphorylates Tyr284 in TGF-beta type II receptor and regulates TGF- $\beta$  stimulation of p38 MAPK during breast cancer cell proliferation and invasion. *Cancer Res.* 2007;67(8):3752-3758.
- Harburger DS, Calderwood DA. Integrin signaling at a glance. *J Cell Sci.* 2009;122(pt 2):159-163.
- Moser M, Legate KR, Zent R, Fassler R. The tail of integrins, talin, and kindlins. *Science.* 2009;324(5929):895-899.
- Borza CM, Pozzi A. The role of cell-extracellular matrix interactions in glomerular injury. *Exp Cell Res.* 2012;318(9):1001-1010.
- Munger JS, et al. The integrin  $\alpha$ v $\beta$ 6 binds and activates latent TGF  $\beta$  1: a mechanism for regulating pulmonary inflammation and fibrosis. *Cell.* 1999;96(3):319-328.
- Mu D, et al. The integrin  $\alpha$ (v) $\beta$ 8 mediates epithelial homeostasis through MT1-MMP-dependent activation of TGF- $\beta$ 1. *J Cell Biol.* 2002;157(3):493-507.
- Khan S, et al. Mesangial cell integrin  $\alpha$ 5 $\beta$ 1 provides glomerular endothelial cell cytoprotection by sequestering TGF- $\beta$  and regulating PECAM-1. *Am J Pathol.* 2011;178(2):609-620.
- Hayashida T, Jones JC, Lee CK, Schnaper HW. Loss of  $\beta$ 1-integrin enhances TGF- $\beta$ 1-induced collagen expression in epithelial cells via increased  $\alpha$ v $\beta$ 3-integrin and Rac1 activity. *J Biol Chem.* 2010;285(40):30741-30751.
- Girgert R, et al. Integrin  $\alpha$ 2-deficient mice provide insights into specific functions of collagen receptors in the kidney. *Fibrogenesis Tissue Repair.* 2010;3:19.
- Gallagher AJ, Schiemann WP.  $\beta$ 3 integrin and Src facilitate transforming growth factor- $\beta$  mediated induction of epithelial-mesenchymal transition in mammary epithelial cells. *Breast Cancer Res.* 2006;8(4):R42.
- Gewin L, Zent R. How does TGF- $\beta$  mediate tubulointerstitial fibrosis? *Semin Nephrol.* 2012;32(3):228-235.
- Ma LJ, et al. Transforming growth factor- $\beta$ -dependent and -independent pathways of induction of tubulointerstitial fibrosis in  $\beta$ 6(-/-) mice. *Am J Pathol.* 2003;163(4):1261-1273.
- Zhang X, et al.  $\beta$ 1 integrin is necessary for ureteric bud branching morphogenesis and maintenance of collecting duct structural integrity. *Development.* 2009;136(19):3357-3366.
- Chen D, et al. Differential expression of collagen- and laminin-binding integrins mediates ureteric bud and inner medullary collecting duct cell tubulogenesis. *Am J Physiol Renal Physiol.* 2004;287(4):F602-F611.
- Chen X, et al. Lack of integrin  $\alpha$ 1 $\beta$ 1 leads to severe glomerulosclerosis after glomerular injury. *Am J Pathol.* 2004;165(2):617-630.
- Gardner H, Broberg A, Pozzi A, Laato M, Heino J. Absence of integrin  $\alpha$ 1 $\beta$ 1 in the mouse causes loss of feedback regulation of collagen synthesis in normal and wounded dermis. *J Cell Sci.* 1999;112(pt 3):263-272.
- Zent R, et al. Glomerular injury is exacerbated in diabetic integrin  $\alpha$ 1-null mice. *Kidney Int.* 2006;70(3):460-470.
- Borza CM, et al. Integrin  $\alpha$ 1 $\beta$ 1 promotes caveolin-1 dephosphorylation by activating T cell protein-tyrosine phosphatase. *J Biol Chem.* 2010;285(51):40114-40124.
- Chen X, et al. Integrin  $\alpha$ 1 $\beta$ 1 controls reactive oxygen species synthesis by negatively regulating epidermal growth factor receptor-mediated Rac activation. *Mol Cell Biol.* 2007;27(9):3313-3326.
- Chen X, et al. Integrin  $\alpha$ 1 $\beta$ 1 regulates epidermal growth factor receptor activation by controlling peroxisome proliferator-activated receptor  $\gamma$ -dependent caveolin-1 expression. *Mol Cell Biol.* 2010;30(12):3048-3058.
- Postigo AA. Opposing functions of ZEB proteins in the regulation of the TGF $\beta$ /BMP signaling pathway. *EMBO J.* 2003;22(10):2443-2452.
- Xiong M, et al. The miR-200 family regulates TGF- $\beta$ 1-induced renal tubular epithelial to mesenchymal transition through Smad pathway by targeting ZEB1 and ZEB2 expression. *Am J Physiol Renal Physiol.* 2012;302(3):F369-F379.
- Xu J, Lamouille S, Derynck R. TGF- $\beta$ -induced epithelial to mesenchymal transition. *Cell Res.* 2009;19(2):156-172.
- Sato M, Muragaki Y, Saika S, Roberts AB, Ooshima A. Targeted disruption of TGF- $\beta$ 1/Smad3 signaling protects against renal tubulointerstitial fibrosis induced by unilateral ureteral obstruction. *J Clin Invest.* 2003;112(10):1486-1494.
- Mattila E, Pellinen T, Nevo J, Vuoriluoto K, Arjonen A, Ivaska J. Negative regulation of EGFR signalling through integrin- $\alpha$ 1 $\beta$ 1-mediated activation of protein tyrosine phosphatase TCPTP. *Nat Cell Biol.* 2005;7(1):78-85.
- Mattila E, Auvinen K, Salmi M, Ivaska J. The protein tyrosine phosphatase TCPTP controls VEGFR2 signalling. *J Cell Sci.* 2008;121(pt 21):3570-3580.
- Mattila E, et al. Inhibition of receptor tyrosine kinase signalling by small molecule agonist of T-cell protein tyrosine phosphatase. *BMC Cancer.* 2010;10:7.
- Zhang S, Chen L, Luo Y, Gunawan A, Lawrence DS, Zhang ZY. Acquisition of a potent and selective T-PTP inhibitor via a stepwise fluorophore-tagged combinatorial synthesis and screening strategy. *J Am Chem Soc.* 2009;131(36):13072-13079.
- Kriegelstein CF, et al. Collagen-binding integrin  $\alpha$ 1 $\beta$ 1 regulates intestinal inflammation in experimental colitis. *J Clin Invest.* 2002;110(12):1773-1782.
- Becker HM, et al.  $\alpha$ 1 $\beta$ 1 integrin-mediated adhesion inhibits macrophage exit from a peripheral inflammatory lesion. *J Immunol.* 2013;190(8):4305-4314.
- Zhu S, et al. Spermine protects mice against lethal sepsis partly by attenuating surrogate inflammatory markers. *Mol Med.* 2009;15(7-8):275-282.
- Meng XM, Chung AC, Lan HY. Role of the TGF- $\beta$ /BMP-7/Smad pathways in renal diseases. *Clin Sci (Lond).* 2013;124(4):243-254.
- Carthy JM, Garmaroudi FS, Luo Z, McManus BM. Wnt3a induces myofibroblast differentiation by upregulating TGF- $\beta$  signaling through SMAD2 in a beta-catenin-dependent manner. *PLoS One.* 2011;6(5):e19809.
- Ren M, et al. Smad2 and Smad3 as mediators of the response of adventitial fibroblasts induced by transforming growth factor  $\beta$ 1. *Mol Med Report.*

- 2011;4(3):561–567.
41. Zhong X, Chung AC, Chen HY, Meng XM, Lan HY. Smad3-mediated upregulation of miR-21 promotes renal fibrosis. *J Am Soc Nephrol*. 2011;22(9):1668–1681.
42. Gewin L, et al. TGF- $\beta$  receptor deletion in the renal collecting system exacerbates fibrosis. *J Am Soc Nephrol*. 2010;21(8):1334–1343.
43. Liu T, Feng XH. Regulation of TGF- $\beta$  signaling by protein phosphatases. *Biochem J*. 2010;430(2):191–198.
44. Bennett D, Alphey L. PP1 binds Sara and negatively regulates Dpp signaling in *Drosophila melanogaster*. *Nat Genet*. 2002;31(4):419–423.
45. Tang WB, Ling GH, Sun L, Liu FY. Smad anchor for receptor activation (SARA) in TGF- $\beta$  signaling. *Front Biosci (Elite Ed)*. 2010;2:857–860.
46. Heikkinen PT, et al. Hypoxia-activated Smad3-specific dephosphorylation by PP2A. *J Biol Chem*. 2010;285(6):3740–3749.
47. Yu J, et al. MTMR4 attenuates transforming growth factor beta (TGF $\beta$ ) signaling by dephosphorylating R-Smads in endosomes. *J Biol Chem*. 2010;285(11):8454–8462.
48. Lin X, et al. PPM1A functions as a Smad phosphatase to terminate TGF $\beta$  signaling. *Cell*. 2006;125(5):915–928.
49. Lorenzen JA, Dadabay CY, Fischer EH. COOH-terminal sequence motifs target the T cell protein tyrosine phosphatase to the ER and nucleus. *J Cell Biol*. 1995;131(3):631–643.
50. Lam MH, Michell BJ, Fodero-Tavoletti MT, Kemp BE, Tonks NK, Tiganis T. Cellular stress regulates the nucleocytoplasmic distribution of the protein-tyrosine phosphatase TCPTP. *J Biol Chem*. 2001;276(40):37700–37707.
51. Soda K, Kano Y, Chiba F, Koizumi K, Miyaki Y. Increased polyamine intake inhibits age-associated alteration in global DNA methylation and 1,2-dimethylhydrazine-induced tumorigenesis. *PLoS One*. 2013;8(5):e64357.
52. Soda K, Kano Y, Chiba F. Food polyamine and cardiovascular disease — an epidemiological study. *Glob J Health Sci*. 2012;4(6):170–178.
53. Goek ON, et al. Metabolites associate with kidney function decline and incident chronic kidney disease in the general population. *Nephrol Dial Transplant*. 2013;28(8):2131–2138.
54. Gardner H, Kreidberg J, Koteliansky V, Jaenisch R. Deletion of integrin  $\alpha$ 1 by homologous recombination permits normal murine development but gives rise to a specific deficit in cell adhesion. *Dev Biol*. 1996;175(2):301–313.
55. Shi M, et al. Enhancing integrin  $\alpha$ 1 inserted (I) domain affinity to ligand potentiates integrin  $\alpha$ 1 $\beta$ 1-mediated down-regulation of collagen synthesis. *J Biol Chem*. 2012;287(42):35139–35152.
56. Yamashita M, Fatyol K, Jin C, Wang X, Liu Z, Zhang YE. TRAF6 mediates Smad-independent activation of JNK and p38 by TGF- $\beta$ . *Mol Cell*. 2008;31(6):918–924.
57. Abe M, Harpel JG, Metz CN, Nunes I, Loskutoff DJ, Rifkin DB. An assay for transforming growth factor- $\beta$  using cells transfected with a plasminogen activator inhibitor-1 promoter-luciferase construct. *Anal Biochem*. 1994;216(2):276–284.